Journal of the Meteorological Society of Japan

EARLY ONLINE RELEASE

The DOI for this manuscript is
DOI:10.2151/jmsj. 2018-026
J-STAGE Advance published date: February 5th, 2018
The final manuscript after publication will replace the preliminary version at the above DOI once it is available.

Aerosol Optical Characteristics in Fukuoka and Beijing Measured by Integrating Nephelometer and Aethalometer: Comparison of Source and Downstream Regions

Akihiro Uchiyama[1], Bin Chen[2,3*], Akihiro Yamazaki[4], Guangyu Shi[2], Rei Kudo[4], Chiharu Nishita-Hara[5], Masahiko Hayashi[5], Ammara Habib[2] and Tsuneo Matsunaga[1]**

1: Center for Global Environmental Research, National Institute for Environmental Studies

2: Institute of Atmospheric Physics (IAP), Chinese Academy of Sciences

3: Collaborative Innovation Center on Forecast and Evaluation of Meteorological Disasters,

Nanjing University of Information Science & Technology

4: Meteorological Research Institute, Japan Meteorological Agency

5: Fukuoka Institute for Atmospheric Environment and Health, Fukuoka University

----

Corresponding authors:

* Chen Bin

Institute of Atmospheric Physics (IAP), Chinese Academy of Sciences

Beijing 100029, CHINA
E-mail: chen_bin@mail.iap.ac.cn
** Uchiyama Akihiro
National Institute for Environmental Studies,
Tsukuba 305-8506, JAPAN
E-mail: uchiyama.akihiro@nies.go.jp

Abstract

The aerosol optical characteristics in the East Asian cities of Fukuoka and Beijing were measured from 2010 to 2014. These long-term season-crossing data were compared to understand the differences between the aerosol characteristics at a source and a downstream region. Previously, few long-term, season-crossing observations have been reported. Using a method developed by one of the present authors, the measurement data were analyzed so that the retrieved optical properties can be more accurate than those obtained in previous studies. Using these data, the aerosol characteristics and their frequency distributions were reliably obtained. In Fukuoka, the annual means of the extinction, scattering, and absorption coefficients C_{ext} (525 nm), C_{sca} (525 nm), and C_{abs} (520 nm) were 74.6, 66.1, and 8.1 Mm^{-1}, respectively, whereas those in Beijing were 412.1, 367.2, and 42.4 Mm^{-1}, respectively. The coefficients in Fukuoka were approximately one-fifth of those in Beijing. The single-scattering albedos ω_0 (525 nm) in Fukuoka and Beijing were 0.877 and 0.868, respectively. The asymmetry factors G (525 nm) in the two cities were 0.599 and 0.656, respectively. The extinction Ångström exponents α_{ext} in the two cities were 1.555 and 0.855, respectively. The absorption Ångström exponents α_{abs} in the two cities were 1.106 and 0.977, respectively. The fine and coarse mode volume fractions in Fukuoka were approximately 80% and 20%, and those in Beijing were both approximately 50% except in the summer.

The C_{ext}, C_{sca}, and C_{abs} showed seasonal variation in both cities. Some other properties showed also seasonal variation. In particular, the seasonal variation in α_{abs} was clear in both cities; it tended to be small in the summer and large in the winter. The frequency distributions of various parameters were also investigated. The frequency of $C_{ext} > 500$ Mm^{-1} in Fukuoka was very low, and large C_{ext} values were recorded more frequently in the spring than in other seasons. In Beijing, $C_{ext} > 1000$ Mm^{-1} values were recorded more frequently, and the frequency of 10 $Mm^{-1} \leq C_{abs} \leq$ 60 Mm^{-1} was high in the spring and summer. Furthermore, $\alpha_{abs} < 1.0$ values were recorded frequently, which cannot be explained by the simple external mixture of absorbing aerosols.

To demonstrate the usefulness of the data obtained in this study, the relationships among α_{abs}, α_{ext}, the volume size distribution, the imaginary part of the refractive index and ω_0 were investigated, and two characteristic cases in Beijing (winter) and Fukuoka (spring) were preliminarily analyzed.

Keywords

Aerosol optical characteristics,

Aerosol extinction coefficient,

Aerosol scattering coefficient,

Aerosol absorption coefficient,

Aerosol single-scattering albedo

Ångström exponent

1. Introduction

Aerosol characteristics are an important factor in Earth's radiation budget, which is influenced by radiatively active gases, aerosols, and clouds. Aerosols change the radiation budget directly by absorbing and scattering solar radiation and indirectly through their role as cloud condensation nuclei (CCNs), thereby increasing cloud reflectivity and lifetime (e.g., Ramanathan et al. 2001, Lohmann and Feichter 2005). The variation in the observed surface solar radiation depends on the presence of clouds, aerosols, and radiatively active gases. Aerosols disturb the solar radiation that reaches Earth's surface. Some aerosols scatter solar radiation and enhance the planetary albedo, whereas others absorb solar radiation and trap energy in the climate system.

These processes are controlled by the aerosol optical properties: the scattering, absorption, and extinction coefficients; the single-scattering albedo (SSA), which is the ratio of the scattering coefficient to the extinction coefficient; and the light scattering phase function. Therefore, the aerosol optical properties are important factors. In the 1970s, the importance of the aerosol optical properties was recognized (Yamamoto and Tanaka 1972), and measurement programs were initiated in several locations, including the South Pole, Mauna Loa, and Point Barrow (McComiskey et al. 2004, Delene and Ogren 2002, Sheridan et al. 2001). Awareness of the effect of aerosols on climate radiative forcing led to an increase in the number of measured variables and measurement sites in the 1990s.

In this study, several aerosol optical characteristics were measured using an integrating nephelometer and an aethalometer in two East Asian cities, Beijing and Fukuoka, from 2010 to 2014. Beijing is a well-known megacity in China whose economic activity has continuously increased over the past 30 years, resulting in increases in the population and number of vehicles. Fukuoka is one of the largest cities in western Japan. In the mid-latitude region, synoptic disturbances move from west to east. This movement causes air masses to also move from west to east, and the observation sites in Japan are thus affected by air originating from the continental area. Therefore, the modification of aerosol characteristics during the transport of aerosols can be investigated by comparing the aerosol characteristics of the source and downstream cities. Furthermore, the aerosol characteristics were better clarified by comparing these two cities.

The Institute of Atmospheric Physics (IAP) of the Chinese Academy of Sciences (CAS) and the Meteorological Research Institute (MRI) of the Japan Meteorological Agency (JMA) have been measuring the aerosol optical properties and the surface downward solar irradiance to investigate the effect of the aerosol optical properties on the surface radiation budget as part of a cooperative Chinese and Japanese science and technology program. In this research program, *in situ* ground-based measurements of the scattering and absorption coefficients have been performed in Beijing and Fukuoka using an integrating nephelometer and an aethalometer.

The objective of this study was to characterize the aerosol optical properties in Beijing and Fukuoka using these measurements. The aerosol optical characteristics can be well understood by comparing the measurements obtained in the two cities. Some previous measurements of the aerosol properties in Beijing have been made over week- to month-long periods of intensive measuring campaigns, but few long-term, season-crossing observations have been reported. A two-year measurement survey by He et al. (2009) is the only season-crossing observation reported thus far. In the present study, measurements were performed over a four-year period. Using these data, the aerosol characteristics and their frequency distributions could be reliably obtained. However, the trends of the optical properties were not investigated, because the four-year measurement period is insufficient for such an investigation.

Section 2 describes the data and methods used in this study, the location of the observation sites, and the calibration of the scattering coefficients. Section 3 gives the monthly means and frequency distributions of the investigated optical properties. In Section 4, the characteristics of the optical properties are classified based on their extinction and absorption Ångström exponents, which are indices of the size distribution and the absorption composition, respectively. Section 5 describes the optical characteristics observed during the winter in Beijing and the spring in Fukuoka. The results are summarized in Section 6.

2. Data and methods

2.1 Instruments and measurement period

The scattering and hemispheric backscattering coefficients were measured using an integrating nephelometer (Aurora 3000, Acoem, Australasia). Using LED light sources, the nephelometer simultaneously measures the scattering coefficients at 450 nm (blue), 525 nm (green), and 635 nm (red). The angle range of the light sources is 9°–170° for total scattering and 90°–170° for hemispheric backscattering. Generally speaking, the inlet temperature is higher than the ambient temperature. Therefore, the relative humidity in the inlet of the nephelometer is lower than that of the outside air. This makes it difficult to measure the scattering coefficient at the outside air temperature and humidity. The effect of hygroscopic growth was removed, and the scattering and hemispheric backscattering coefficients were measured under dry conditions. The inlet of the nephelometer has a processor-controlled automatic heater, and the relative humidity threshold was set to 30%. It was confirmed that the relative humidity in the inlet was less than 30%. The instrument was operated at a flow rate of approximately 5 L/min (nominal value).

The absorption coefficients were measured using an aethalometer (Model AE31, Magee Scientific, USA) at seven wavelengths: 370, 450, 520, 590, 660, 880, and 950 nm. The aethalometer measured the attenuation of a beam of light transmitted through the sample collected on a quartz fiber filter while the filter continuously collected samples. The instrument was operated at a flow rate of 1 L/min in Beijing and 4 L/min in Fukuoka. Since aerosol concentration in Beijing was high, we reduced the flow rate so that the aethalometer operated stably. The absorption coefficient can be accurately measured using the recently developed photoacoustic method (Arnott et al. 1999) or the photothermal interferometric method (Sedlacek and Lee 2007). However, filter-based instruments were used because of their stability and ease of operation. Most filter-based absorption coefficient techniques suffer from various systematic errors that require correction (Coen et al. 2010, Weingartner et al. 2003, Arnott et al. 2005, Schmid et al. 2006, Virkkula et al. 2007). All of the scattering and absorption coefficient data were recorded as 1-min averages, and 30-min averaged data were used for data analysis.

The scattering and absorption coefficients were observed over a period of four years in each location: from March 2010 to February 2014 in Beijing and from August 2010 to May 2014 in Fukuoka. In the period from March 2010 to September 2011 in Beijing, the nephelometer was used without hemispheric backscattering measurements. Although the details are not described here, the differences between the analyzed results with and without hemispheric backscattering measurements were small.

In June 2011, the light source of the nephelometer installed in Fukuoka was discovered to be malfunctioning. During the period from the middle of January to June

2011, the extinction Ångström exponents α_{ext} were very large in comparison with those from other periods. Based on this unusual discrepancy, it was assumed that the light source began to malfunction in the middle of January. Therefore, the data from this period were not used, and the measurement was restarted in January 2012. During the period from July 2012 to February 2013 in Beijing, all instruments were stopped while the room where the instruments were installed underwent renovation.

2.2 Observation sites

The aerosol optical properties were measured in Beijing, China, and Fukuoka, Japan, the locations of which are shown in Fig. 1(a). Beijing is located in the area bordering the North China Plain and the Inner Mongolia plateau and is surrounded by the Taihang Mountains to the west and the Yanshan Mountains to the north. Beijing is a megacity with a population of more than 21,500,000. The measurements were made at the IAP (116.38° E, 39.97° N), which is located in the northern part of the urban area of Beijing. The IAP is surrounded by a number of research institutes and residential and business complexes, and there are no factories nearby. The instruments were installed in a room on the roof approximately 35 m from the ground and 92 m above sea level. Sample air from outside the building was drawn into the instrument through an electric conductive tube passed through a window. The length of tube was approximately 1.5 m, and the tube was connected to an isokinetic inlet. This inlet is no size-selective. The sample air was branched and guided to each instrument. It was confirmed that the instruments did not interfere with each other. The room was not air conditioned.

Fukuoka is located on the northern shore of the island of Kyushu, facing the Sea of Japan, and is surrounded by the Sefuri Mountains to the south and southwest. Fukuoka is Kyushu's largest city with a population of approximately 1,500,000. The measurements for this study were conducted at Fukuoka University Campus (130.36° E, 33.55° N), which is located in the western part of the urban area of Fukuoka approximately 6 km from the sea and 1.5 km from the mountains. The university is surrounded by a number of residential quarters, and there are no factories nearby. The instruments were installed in a room on the fourth floor, approximately 15 m from the ground and 23 m above sea level. Sample air from outside the building was drawn into the instrument through an electric conductive tube passed through a window. The length of tube was approximately 1.5 m. As in Beijing, the tube was connected to an isokinetic inlet. This inlet is no size-selective. It was also confirmed that the instruments did not interfere with each other. The room was air-conditioned to maintain a temperature of 25 °C.

During the observation periods, some construction was done near both observation sites, which may have affected the measurements.

2.3 Calibration of instruments

The nephelometer is able to regularly monitor the output of the instrument by measuring calibration gases without changing the calibration coefficients. Filtered air and CO_2 gas were used for the zero check and span check operations, respectively. The calibration check of the nephelometer was performed once per week at midnight. Correction coefficients were calculated from the calibration check data after each calibration check, and a quadratic function of time was fit to these coefficients using the method of least squares.

The aethalometer did not require special calibration, because it measures transmittance, which is a relative value. An important factor that influences measurement precision is the flow rate because it determines the sampling volume. The flow rate was measured using a precision soap film flow meter and compared with the recorded values; these measured flow rates were within 0.5% of the recorded values.

2.4 Data processing method

Filter-based instruments are widely used at ground sites. However, most filter-based absorption coefficient techniques suffer from various systematic errors that require correction (Liousse et al. 1993, Petzold et al. 1997, Bond et al. 1999, Weingartner et al. 2003, Arnott et al. 2005, Schmid et al. 2006, Virkkula et al. 2007, Coen et al. 2010). In this study, the method by Coen et al. (2010) was used. Their correction scheme is based on four previously published methods that account for the optical properties of the aerosol particles embedded in the filter (Weingartner et al. 2003, Arnott et al. 2005, Schmid et al. 2006, Virkkula et al. 2007). Because multi-wavelength scattering coefficient data can be used, the performance of the correction method developed by Coen et al. (2010) is expected to be very good.

Integrating nephelometers are widely used to measure aerosol scattering coefficients; however, they cannot measure light scattered in extreme forward or backward directions (scattering angles near 0° and 180°; Heintzenberg and Charlson 1996, Anderson et al. 1996, Anderson and Ogren 1998, Müller et al. 2009). To correct for this truncation error, information on aerosol absorption properties and the particle size distribution is necessary (Bond et al. 2009). This study employed a recently developed method that uses multi-wavelength scattering and absorption coefficient data to correct the scattering coefficients (Uchiyama 2014, see Supplement 1).

2.5 Backward trajectory

To determine the characteristics of air masses during each season, backward trajectory analysis was conducted starting at a height of 500 m above the observation sites every 4 h from 2004 to 2013 in Fukuoka and from 2008 to 2013 in Beijing. These data were used to clarify the seasonal variation in the aerosol properties. When considering the seasonal variation of the aerosol characteristics, the resident time, which is the time an air mass spends within a given region before reaching the target city, was calculated from the backward trajectory data. The backward trajectory analysis was performed using the Hybrid Single-Particle Lagrangian Integrated Trajectory (HYSPLIT) model (Draxler 1999).

3. Aerosol properties

This section presents the time series, monthly and annual means, and frequency distributions of the aerosol properties. The extinction, scattering, absorption coefficients, the SSA, and the absorption Ångström exponent among aerosol properties are described in detail. The asymmetry factor, the extinction Ångström exponent, and the volume fraction of coarse and fine mode are briefly described and shown in detail in the Supplement 2.

3.1 Extinction, scattering, and absorption coefficients

First, the measured extinction, scattering, and absorption coefficients C_{ext}, C_{sca}, and C_{abs} are discussed. Figures 2(a) and (b) show the time series of the monthly mean scattering and absorption coefficients and their standard deviations. The monthly and annual mean values of the aerosol properties are given in Tables 1 and 2. As shown later, the frequency distributions of the aerosol properties deviate considerably from the normal distribution, but the mean value and the standard deviation are expressed in the form of the mean ± standard deviation.

In Fukuoka, the annual means and standard deviations of C_{ext}, C_{sca}, and C_{abs} at wavelengths of 525, 525, and 520 nm, respectively, during the period from August 2010 to May 2014 were 74.6 ± 52.9, 66.1 ± 48.4, and 8.1 ± 5.3 Mm^{-1}, respectively (Table 1). In Beijing, the annual means of the same coefficients during the period from March 2010 to February 2014 were 412.1 ± 462.6, 367.2 ± 424.4, and 42.4 ± 37.5 Mm^{-1}, respectively (Table 2). The annual mean coefficients C_{ext} (525 nm), C_{sca} (525 nm), and C_{abs} (520 nm) in Fukuoka were approximately one-fifth of those in Beijing and were slightly larger than the coefficients in Tsukuba, Japan: C_{ext} (550 nm) = 62.8 Mm^{-1}, C_{sca} (550 nm) = 55.2 Mm^{-1}, and C_{abs} (530 nm) = 7.5 Mm^{-1} (Uchiyama et al. 2014).

Some previous measurements of the aerosol optical properties in Beijing were made over week- to month-long periods of intensive measuring campaigns (Bergin et al. 2001, Yan et al. 2008, Li et al. 2007, Garland et al. 2009), but few long-term, season-crossing observations have been reported (Table 3). He et al. (2009) studied the aerosol optical properties in Beijing using two-year data. According to He et al. (2009), the two-year averages and standard deviations for C_{abs} (532 nm) and C_{sca} (525 nm) were 56 ± 49 and 288 ± 281 Mm^{-1}, respectively. The extinction coefficient with no wavelength correction was approximately $C_{ext} \approx C_{sca} + C_{abs}$ = 288 Mm^{-1} + 56 Mm^{-1} =

344 Mm^{-1}. The value of C_{abs} obtained in the present study is smaller than that obtained in their study, and the values of C_{ext} and C_{sca} in the present study are larger than those obtained in their study. However, because the standard deviations are very large in Beijing, it is difficult to determine whether there is a significant difference between the present results and those obtained by He et al. (2009). Table 3 also gives measurement values that have been reported in other previous studies. Because these measurements were not conducted during the same time periods, it is difficult to compare the long- and short-period data.

Figures 2(a) and (b) and Tables 1 and 2 show the seasonal variation in C_{ext}, C_{sca}, and C_{abs}; in the summer, these coefficients were small, whereas in the winter, they were large. The seasonal variation in Fukuoka was more distinct than that in Beijing.

To investigate the characteristics of the air masses in every season, the resident time was calculated using the results of the backward trajectory analysis. The study area was divided into eight regions, and the area outside of East Asia was classified as the outside region (Fig. 1(b)). Tables 4 and 5 give the frequency with which each region had the longest resident time during the five days prior to the air mass arriving in the target city. The backward trajectory was analyzed monthly to determine these frequencies.

The results of the backward trajectory analysis also yielded the seasonal variation of the origins of the air masses arriving in the two target cities. Most air masses that reached Fukuoka in the summer, winter, and spring were affected by the West Pacific Ocean region (region 8), the North Continent region (region 1), and the North Continent and Japan regions (regions 1 and 6), respectively. Most air masses that reached Beijing from November to April and May to October were affected by the North Continent region (region 1) and the East China region (region 3), respectively.

The seasonal variation in C_{ext}, C_{sca}, and C_{abs} in Beijing is unclear. The coefficient values in autumn and winter were large. He et al. (2009) found that C_{ext} and C_{sca} were largest in the summer (Table 2 in their paper). However, according to the present results, the coefficients were not necessarily large in the summer. The results of the sky radiometer analysis by Che et al. (2014) showed that the optical thickness was largest in the summer and smallest in the winter. Sky radiometer measurements cannot be made in very hazy conditions because the direct solar irradiances cannot be measured, making it difficult to distinguish between clouds and heavy haze. Therefore, the average value in the winter was weighted by the results from days with light haze. As shown in Fig. 2(b), C_{sca} and C_{abs} varied drastically in the winter in Beijing.

Figures 2(c), (d), (e) and (d) show the frequency distributions of C_{ext} and C_{abs} for each season, where spring, summer, autumn, and winter are defined as March–May, June–August, September–November, and December–February, respectively. In Fukuoka, most measured C_{ext} values were less than 500 Mm^{-1}, and the most frequently recorded values of C_{ext} were less than 100 Mm^{-1}. However, relatively large C_{ext} values were observed in the spring. In Beijing, values of C_{ext} larger than 1000 Mm^{-1} were frequently observed. The most frequently recorded values of C_{ext} were less than 100 Mm^{-1}, and values between 100 and 500 Mm^{-1} were recorded more frequently in the spring and summer.

In Fukuoka, relatively large values of C_{abs} and C_{ext} were observed in the spring, and larger values of C_{abs} were observed less frequently in the summer. In Beijing, the most frequently recorded value of C_{abs} in the spring was 25 Mm^{-1}, and a second smaller peak in the summer frequency distribution also occurred at C_{abs} = 10 Mm^{-1}, as shown in Fig. 2(f). In the other seasons, the most frequently recorded values were C_{abs} < 10 Mm^{-1}. The percentage of recorded values between 10 and 60 Mm^{-1} was high in the spring and the summer, and this feature was particularly distinctive in the summer. In the autumn and winter, C_{abs} exceeded 100 Mm^{-1} relatively frequently.

3.2 Single-scattering albedo

Figures 3(a) and (b) show the time series of the monthly mean SSAs (ω_0) and their standard deviations at a wavelength of 525 nm. Tables 1 and 2 give the monthly and annual means of ω_0 (525 nm). The scattering coefficients were properly corrected using the new method.

ω_0 (525 nm) in Fukuoka ranged from 0.75 to 0.95, and its annual mean value was 0.877 ± 0.053. As shown in Figs. 3(a) and (b), ω_0 (525 nm) in Fukuoka underwent seasonal variation; it was large in the spring and small in the autumn. ω_0 (525 nm) in Beijing ranged from 0.75 to 0.95, which is similar to the range in Fukuoka, and its annual mean was 0.868 ± 0.047. The variation of ω_0 (525 nm) in Beijing did not follow a clear seasonal trend, but ω_0 (525 nm) did change greatly from year to year.

The average SSA obtained by He et al. (2009) was 0.80 ± 0.09, which is smaller than the average SSA measured in the present study. As shown in Supplement 2, the Ångström exponent for the extinction coefficient in Beijing was small throughout the year. This indicates that the measured aerosols included numerous large particles and that the scattering coefficients measured by the integrating nephelometer required a large correction. He et al. (2009) did not mention the correction of scattering coefficient. The use of the corrected SSA provides the explanation of most of the difference between present results and those obtained by He et al. (2009). (see Supplement 3.)

Che et al. (2014) analyzed sky radiometer (POM-02, Prede, Japan) data from Beijing and obtained seasonal average SSAs ranging from 0.93 to 0.96. These values are larger than the SSAs measured in the present study. The SSAs estimated from the sky radiometer measurements are column-averaged SSAs of aerosols under ambient conditions, which involve hygroscopic growth. The ground-based measurements in the present study were conducted under dry air conditions. Because the two measurements were conducted under different conditions, comparisons between the results of ground-based and sky radiometer measurements must be made carefully.

Figures 3(c) and (d) show the frequency distribution of ω_0 (525 nm) for every season. In Fukuoka, the most frequent value in the spring was 0.915, and the width of the frequency distribution in the spring was narrower than that in the other seasons. Most SSAs recorded in the spring were more than 0.8. In the other seasons, a larger percentage of recorded SSAs were less than 0.8. In Fukuoka, the peak of the frequency distribution in the summer was broad, and lower SSAs were observed. In the summer, Fukuoka was mainly covered with air masses that originated in the West Pacific Ocean region (region 8), which are typically clean. Most light-absorbing aerosols present in Fukuoka were emitted from local sources, and their seasonal variation is small. Therefore, the relative contribution of C_{abs} to C_{ext} was high in the summer, and lower SSAs were observed.

In Beijing, the most frequently recorded ω_0 (525 nm) values were 0.895 in the spring, 0.905 in the summer, and 0.885 in the autumn and winter. The frequency distribution in the winter was narrower than those in the other seasons. In the summer, lower SSAs were observed more frequently than in the other seasons. The reason for this is that the most frequently recorded C_{abs} in summer was 25 Mm^{-1}, which is larger than those in the other seasons.

3.3 Asymmetry factor, extinction Ångström exponent and volume fraction

The results on the asymmetry factor G, extinction Ångström exponent α_{ext}, and volume fraction of coarse and fine mode are briefly shown in this section. The details on these parameters are shown in the Supplement 2.

Tables 1 and 2 give the monthly and annual means of these parameters and their standard deviations.

G (525 nm) in Fukuoka ranged from 0.5 to 0.7, and its annual mean was 0.599 ± 0.040. G (525 nm) in Beijing ranged from 0.6 to 0.75, and the annual mean was 0.656 ± 0.042. No clear seasonal variation was observed in the both cities. G (525 nm) in Beijing was larger than that in Fukuoka.

The α_{ext} values in Fukuoka ranged from 1.0 to 2.1. The annual mean was 1.555 ± 0.312. The α_{ext} values in Beijing ranged from 0.2 to 1.5, and the annual mean was 0.855 ± 0.347. α_{ext} in Beijing was smaller than that in Fukuoka by approximately 0.7.

The aerosol volume was obtained by integrating the retrieved volume size distribution. The volume was then divided into two parts: fine and coarse mode volumes (V_f and V_c) with particle radii less and greater than 0.5 μm, respectively. The V_c in Beijing was larger than that in Fukuoka. In Fukuoka, the V_f was approximately 80%. In Beijing, V_c was approximately 60% in the autumn and winter, and both V_f and V_c were approximately 50% in the spring and summer.

The larger asymmetry factor in Beijing, the smaller α_{ext} in Beijing and the larger V_c in Beijing than in Fukuoka are consistent. These results mean that in Beijing, the particles present in the air were coarser than those in Fukuoka.

3.4 Absorption Ångström exponent

The wavelength dependence of the absorption coefficient can be approximated by an equation similar to that relating C_{ext} and α_{ext}:

$$C_{abs} \propto \lambda^{-\alpha_{abs}},$$

where α_{abs} is the absorption Ångström exponent, which is dependent on the aerosol composition and aging stage (Russell et al. 2010, Clarke et al. 2007). The characteristics of α_{abs}, which have not been investigated in previous studies, are discussed here. Furthermore, the relationships between α_{abs} and other parameters are described in a later section.

Figures 4(a) and (b) show the time series of the monthly means of α_{abs} with their standard deviations. Tables 1 and 2 give the monthly and annual means of α_{abs}. As shown in Figs. 4(a) and (b), α_{abs} demonstrated remarkable seasonal variation in both Fukuoka and Beijing; α_{abs} was small in the summer and large in the winter. Most α_{abs} values ranged from 0.6 to 1.5. The annual means of α_{abs} were 1.106 ± 0.155 in Fukuoka and 0.977 ± 0.147 in Beijing. The values of α_{abs} in Beijing were slightly smaller than those in Fukuoka.

Figures 4(c) and (d) show the frequency distributions of α_{abs} during each season in Fukuoka and Beijing. The most frequently recorded values varied seasonally. The monthly mean α_{abs} in the summer in Fukuoka was approximately 1.0, which usually indicates that the absorbing aerosol is composed mainly of fresh black carbon. However, the frequency distribution in the summer demonstrates that α_{abs} values below 1.0 were observed frequently. In Beijing, the monthly mean α_{abs} values in the summer were less than 1.0, and the frequency distribution also demonstrates the existence of aerosols with $\alpha_{abs} < 1.0$.

Russell et al. (2010) conducted measurements using the Aerosol Robotic Network (AERONET) and found α_{abs} values near 1 (the theoretical value for fresh black carbon) for aerosol columns dominated by urban–industrial aerosols, larger α_{abs} values for biomass burning aerosols, and the largest α_{abs} values for Sahara dust aerosols. These are typical light-absorbing aerosols, which have α_{abs} values greater than or equal to 1. Therefore, a simple external mixture of these aerosols cannot explain an α_{abs} value of less than 1.

Gyawali et al. (2009) observed biomass burning aerosols with $\alpha_{abs} < 1.0$ and demonstrated that such values of α_{abs} can result from black carbon coated with either absorbing or non-absorbing material. Bergstrom et al. (2007) noted that the interesting observation of $\alpha_{abs} < 1.0$ may be the result of measurement uncertainties or somewhat large values of the imaginary part of the refractive index (ImRF) at longer wavelengths for certain particles. Additionally, very low values of α_{abs} have been reported under different circumstances without explanation (Bergstrom et al. 2007, Clarke et al. 2007, Roden et al. 2006, Subramanian et al. 2007, Yang et al. 2009). Because α_{abs} values below 1.0 were observed in both Fukuoka and Beijing, future studies must explain what conditions cause α_{abs} to be less than 1.0.

Tables 1 and 2 give the monthly and annual means of the absorption Ångström exponents α_{abs_sw} in the region of wavelengths shorter than 520 nm and α_{abs_lw} in the region of wavelengths longer than 590 nm, which also showed seasonal variation. It is known that brown carbon shows stronger absorption characteristics in the ultraviolet (UV) region than in the visible light region (Moosmüller et al. 2009). However, it is very difficult to interpret α_{abs_sw} and α_{abs_lw} data, and thus only the values are given in this study.

As shown in Tables 1 and 2, when α_{abs_sw} and α_{abs_lw} are similar to each other, α_{abs} is smaller than both α_{abs_sw} and α_{abs_lw}. This indicates that the absorption coefficient is not a monotonically decreasing function of the wavelength; the absorption coefficients in the region of wavelengths between 520 and 590 nm are constant or have small peak with respect to the wavelength. The cause of this wavelength dependence remains unclear; its determination would require further study of the absorption coefficient of aerosols.

4. Optical properties classified by extinction and absorption Ångström exponents

α_{ext} is an index of the size distribution, and α_{abs} is related to the aerosol components (Russell et al. 2010). Therefore, the data in this study were classified using these parameters, and the relationships between these parameters and the aerosol optical properties were investigated. The relationships between α_{abs} and other parameters have not been investigated in previous studies. Classifications based on α_{ext} and α_{abs} have already been conducted by Russell et al. (2010) and Clarke et al. (2007). Russell et al. (2010) classified absorbing aerosols as desert dust, urban industrial, and biomass burning aerosols. Clarke et al. (2007) classified aerosols observed on aircraft as dust, biomass burning, and pollution plume aerosols.

Figure 5 shows scatter plots of α_{ext} and α_{abs}. The data used in these plots are one-day averages, and there are no distinct clusters. It appears to be difficult to classify these data based on the magnitudes of α_{ext} and α_{abs}. In Fukuoka and Beijing, the data were clustered around (α_{ext}, α_{abs}) = (1.5, 1.1) and (1.0, 1.0), respectively. Both α_{ext} and α_{abs} in Fukuoka were slightly larger than those in Beijing. There was weak positive correlation between α_{ext} and α_{abs} in both cities.

4.1 Absorption Ångström exponent and volume size distribution

To investigate the relationship between α_{abs} and the volume size distribution, the data were classified according to α_{abs} using the following bins: 0.2–0.4, 0.4–0.6, 0.6–0.8, 0.8–1.0, 1.0–1.2, 1.2–1.4, and 1.4–1.6. This relationship between α_{abs} and the volume size distribution has not been discussed in previous studies. Figure 6 shows the volume size distribution classified by α_{abs}. As indicated in the scatter plot of α_{abs} and α_{ext}, when α_{abs} is small, the aerosol contains many large particles. This feature was observed in both Fukuoka and Beijing. The difference between the distributions in Fukuoka and Beijing was caused by differences in α_{ext}; α_{ext} in Beijing was smaller than that in Fukuoka, and the aerosols in Beijing thus contained larger particles.

4.2 Extinction Ångström exponent and volume size distribution

To investigate the relationship between α_{ext} and the volume size distribution, the data were classified according to α_{ext} using the following bins: −0.5–0.5, 0.5–1.0, 1.0–1.5, 1.5–2.0, 2.0–2.5, and 2.5–3.0. Figure 7 shows the volume size distribution classified by α_{ext}. For $\alpha_{ext} < 1$, the retrieved volume size distributions were bimodal with peaks at radii of approximately 0.1 and 2.0 μm, and for $\alpha_{ext} > 1$, the volume size distributions were monomodal with a peak at a radius of approximately 0.1 μm. These peaks at radii of approximately 0.1 and 2.0 μm correspond to the accumulation and coarse particle modes, respectively. Similar results were reported at Tsukuba by Uchiyama et al. (2014).

4.3 Absorption Ångström exponent and imaginary part of refractive index

The ImRF was also determined using the analysis method developed by one of the present authors (Uchiyama 2014). The relationships between the ImRF and other parameters were thus investigated.

To investigate the relationship between α_{abs} and the ImRF, the data were classified according to α_{abs}. Because the dependence of the real part of the refractive index on α_{ext} and α_{abs} is small, the dependence of only the ImRF on α_{abs} and α_{ext} is discussed in this study. Figure 8 shows the wavelength dependence of the ImRF; dashed lines indicate few data points. In Fukuoka and Beijing, the ImRF shows a different tendency for the same α_{abs} value. As shown in Fig. 6, the size distributions in the two cities at the same α_{abs} value differed from each other. These differences in the size distribution caused the different tendencies in the ImRF. Roughly speaking, when α_{abs} is small, the ImRF tends to be small. In Fukuoka, the ImRF increased with increasing wavelength. When α_{abs} was large, the ImRF tended to be large. However, in Beijing, the ImRF decreased with increasing wavelength.

As mentioned in Section 3.4, Russell et al. (2010) obtained α_{abs} values near 1 (the theoretical value for fresh black carbon) for aerosol columns dominated by urban–industrial aerosols, larger α_{abs} values for biomass burning aerosols, and the largest α_{abs} values for Sahara dust aerosols. In addition, according to the simulation results obtained by Gyawali et al. (2009) based on the coated sphere model, α_{abs} is less than 1.0 for aerosols coated with light absorbing or non-absorbing aerosols with relatively large cores and increases with increasing coating thickness for aerosols with relatively small cores. Furthermore, the figures in Gyawali et al. (2009) (Figs. 8 and 9 in their paper) show that if the light-absorbing aerosol coating is thick, α_{abs} is greater than 1.0 regardless of the size of the core. This also indicates that α_{abs} is greater than 1.0 for large light-absorbing aerosols. It was also found that α_{abs} is less than 1.0 for aerosols coated with non-light-absorbing aerosols with relatively large cores.

When α_{abs} is small, the ImRF is small, and the fraction of coarse particles is high, as shown in Fig. 6. Because the ImRF is small, the aerosol contains many non-absorbing components either through external or internal mixing. Sea salt particles, internally mixed particles rich in non-light-absorbing components, and aerosols that have undergone hygroscopic growth are conceivable as coarse and non-light-absorbing aerosols. According to the simulation results obtained by Gyawali et al. (2009), if the aerosol has a relatively large core and is coated with a non-light-absorbing aerosol, α_{abs} is less than 1.0. This aerosol model is consistent with the present measurement results. Although the relative humidity in the nephelometer inlet was maintained at 30% or less, it is also possible that the hygroscopically grown aerosols, which consisted of internally mixed light-absorbing aerosols, passed through the inlet of the nephelometer before they were sufficiently dried.

In Fukuoka, when α_{abs} was large, the volume size distribution was monomodal (Fig. 6(a)), the fraction of fine particles was high, and α_{ext} was large. In contrast, in Beijing, when α_{abs} was large, the volume size distribution was bimodal (Fig. 6(b)), the fraction of coarse particles was high, and α_{ext} was small. As shown in the simulation results obtained by Gyawali et al. (2009), in Fukuoka, aerosols coated with light-absorbing or non-light-absorbing aerosols with relatively small cores may include fine light-absorbing aerosols; i.e. black carbon coated with secondary species like organic matter, and nitrate or sulfate species from gas-to-particle conversion. In Beijing, α_{abs} was large, and α_{ext} was small. The ImRF was large and decreased with increasing wavelength. These features are similar to those of mineral dust.

4.4 Extinction Ångström exponent and imaginary part of refractive index

To investigate the relationship between α_{ext} and the ImRF, the data were classified according to α_{ext}. Figure 9 shows the wavelength dependence of the ImRF; dashed lines indicate few data points. When α_{ext} was small ($-0.5 \leq \alpha_{ext} \leq 0.5$), the ImRF was small and decreased with increasing wavelength in both Fukuoka and Beijing. At medium values of α_{ext} ($1.0 \leq \alpha_{ext} \leq 2.0$), the ImRF was large in both Fukuoka and Beijing. For large α_{ext} ($2.0 \leq \alpha_{ext} \leq 3.0$), though few data points were available, the ImRF tended to be small in Beijing and large in Fukuoka.

When α_{ext} is small, the fraction of coarse particles is high. The following two cases are considered as a case where α_{ext} is small. One is the case of mineral dust aerosol. The other is a case where α_{abs} is small. The mineral dust aerosol is characterized by small α_{ext} and large α_{abs}. Additionally, when α_{abs} is small, the fraction of coarse particles is high, as stated in Section 4.1. The ImRF for mineral dust is large in the short visible wavelength region and decreases with increasing wavelength. The ImRF for aerosols with small α_{abs} is small (see Section 4.3). Because the data are not distinguished by the size of α_{abs} in Fig. 9, ImRF shows the average feature of aerosols with small and large α_{abs}; the ImRF was smaller than that of mineral dust aerosols and decreased with increasing wavelength.

In Beijing, when α_{ext} was large, the size distribution was monomodal, as shown in Fig. 7(b). Therefore, the aerosols did not include mineral dust particles. The ImRF in the shorter wavelength region was large and decreased with increasing wavelength. Brown carbon has such characteristics, but because few data points were obtained, it was difficult to make a definitive conclusion.

4.5 Single-scattering albedo and extinction and absorption Ångström exponents

To investigate the relationships among ω_0, α_{ext}, and α_{abs}, the data were roughly divided into the following bins according to the value of C_{ext}: 1–25, 25–100, 100–1000, and 1000–5000 Mm^{-1}. The data were then classified according to α_{abs} and α_{ext}. Tables 6 and 7 give ω_0 (525 nm), and the cells are colored according to the value of ω_0 (525 nm); blue and red cells correspond to high and low values, respectively, and cells with few data points are not colored. Roughly speaking, as C_{ext} increased, ω_0 (525 nm) tended to increase. At large α_{ext} and small α_{abs} (upper right of Tables 6 and 7) and at small α_{ext} and large α_{abs} (lower left of Tables 6 and 7), ω_0 (525 nm) tended to be large.

Large α_{ext} values indicate that the fraction of small particles is high. Therefore, the former case corresponds to newly produced and grown particles, including weakly absorbing or nonabsorbing aerosols such as sulfate particles. Small α_{ext} values indicate that the fraction of large particles is high. Therefore, the latter case corresponds to mineral dust. When both α_{ext} and α_{abs} were large, ω_0 (550 nm) was small. This may correspond to newly produced and grown particles, including absorbing secondary organic aerosols such as brown carbon. However, this region contains few data points (fewer than 5). Therefore, strong conclusions cannot be drawn regarding cases with large values of both α_{ext} and α_{abs}.

5. Case studies

To demonstrate the usefulness of the data obtained in this study, two characteristic cases in Beijing (winter) and Fukuoka (spring) were preliminarily analyzed.

5.1 Optical properties during winter in Beijing

As discussed in Section 3, the winter in Beijing is characterized by very large variation in C_{ext} and C_{abs}; both very clean and very hazy conditions were observed. Although plots of the time series of C_{ext} and C_{abs} are not shown here, after air masses in the North Continent region (region 1) reached Beijing, the air became very clean, resulting in low C_{ext} and C_{abs} values. Then, the air gradually became turbid with daily variation, causing the C_{ext} and C_{abs} values to gradually increase. As C_{ext} and C_{abs} increased, the characteristics of the aerosols changed.

To investigate the changes in the optical properties as the conditions changed from clean to hazy, the data were divided into the following bins according to C_{ext}: 1–25, 25–50, 50–100, 100–200, 200–400, 400–800, 800–1600, and 1600–5000 Mm^{-1}. Figure 10 shows the relationship between the aerosol properties and C_{ext}.

As shown in Fig. 10(a), when C_{ext} was very small (C_{ext} < 25 Mm^{-1}), the wavelength dependence of the SSA was large, and in the middle range of C_{ext} (25 Mm^{-1} ≤ C_{ext} ≤ 200 Mm^{-1}), the wavelength dependence was small. As C_{ext} increased, the SSAs increased, and the wavelength dependence decreased. As shown in Fig. 10(b), *G* decreased with increasing C_{ext} and was smallest in the range of 200 Mm^{-1} ≤ C_{ext} ≤ 400 Mm^{-1}. Then, as C_{ext} increased beyond 400 Mm^{-1}, the asymmetry factors increased again. As shown in Fig. 10(c), α_{ext} was smallest when C_{ext} was small. As C_{ext} increased, α_{ext} was maximized in the range of 200 Mm^{-1} ≤ C_{ext} ≤ 400 Mm^{-1} and then decreased. α_{ext} depends on V_f and V_c, and its change is consistent with the change in *G*.

As shown in Fig. 10(d), α_{abs} was also smallest when C_{ext} was small. As C_{ext} increased, α_{abs} was maximized in the range of 200 Mm^{-1} ≤ C_{ext} ≤ 800 Mm^{-1} and then decreased. The maximum α_{abs} value was approximately 1.2. As shown in Fig. 10(d), when C_{ext} was small, α_{abs_lw} and α_{abs_sw} were approximately 1.0. α_{abs_sw} was maximized in the range of 200 Mm^{-1} ≤ C_{ext} ≤ 400 Mm^{-1} and was approximately 1.35. α_{abs_lw} was maximized in the range of 400 $Mm^{-1} \leq C_{ext} \leq 800$ Mm^{-1} and was approximately 1.15 in this range. The absorption characteristics of brown carbon tend to be stronger in the UV region; α_{abs_sw} was large in the shorter wavelength region (Moosmüller et al. 2009). The observed features in the range of 200 $Mm^{-1} \leq C_{ext} \leq 800$ Mm^{-1} showed characteristics similar to those of brown carbon. As demonstrated by the variation in α_{ext} and G, V_f and V_c were approximately 50% in the middle range of C_{ext} (200 $Mm^{-1} \leq C_{ext} \leq 400$ Mm^{-1}), and when C_{ext} was smaller or larger, V_f was low and V_c was high, as shown in Fig. 10(e).

These changes in the aerosol characteristics due to changes in the aerosol amount indicate that as air masses from the North Continent region (region 1) reached Beijing, the air became clean, C_{ext} gradually increased, and the aerosol characteristics changed because of the local formation and emission of anthropogenic aerosols and their aging. As the number of pollution particles increased, there was a period when the number of smaller particles increased and α_{ext} became large. Following this period, as the amount of air pollution increased, the number of larger particles increased, and α_{ext} became small. In the former period, new particle formation and condensation likely dominated, and in the latter period, coagulation may have occurred. α_{abs} in the former period was larger than that in the latter period.

The analysis in this study is limited because only the optical properties were considered. To better understand processes related to aerosols, it is necessary to make comprehensive measurements in future works, including measurements of precursor gases, the aerosol composition, the mixing state, and the size distribution.

5.2 Optical properties during spring in Fukuoka

As discussed in Section 3, the spring in Fukuoka was characterized by relatively large C_{ext} and C_{abs} values. Although plots of the time series of C_{ext} and C_{abs} are not shown here, C_{ext} (525 nm) and C_{abs} (520 nm) changed periodically with the passage of a synoptic-scale disturbance. As with the case of the winter in Beijing, the data were divided into bins according to C_{ext} to investigate the dependence of the optical properties on C_{ext}. The bins were the same as those used for Beijing, but no data with C_{ext} > 800 Mm^{-1} were observed: 1–25, 25–50, 50–100, 100–200, 200–400, and 400–800 Mm^{-1}.

Figure 11 shows the relationship between the aerosol properties and C_{ext}. Very few data had C_{ext} > 400 Mm^{-1}. The dependence of the optical properties on C_{ext} differed from that during the winter in Beijing. When C_{ext} was very small (C_{ext} < 25 Mm^{-1}), the wavelength dependence of the SSA was large. As shown in Fig. 11(a), when C_{ext} increased, the SSAs increased monotonically, and the wavelength dependence decreased. As shown in Fig. 11(b), G was somewhat low in the range of 50 Mm^{-1} ≤ C_{ext} ≤ 100 Mm^{-1}. For C_{ext} > 200 Mm^{-1}, G was high. Additionally, as shown in Fig. 11(c), α_{ext} was somewhat high in the range of 50 Mm^{-1} ≤ C_{ext} ≤ 100 Mm^{-1} and decreased in the range of C_{ext} > 200 Mm^{-1}. The dependence of α_{ext} on C_{ext} was consistent with that of G.

As C_{ext} increased, α_{abs} increased, reached a maximum in the range of 50 $Mm^{-1} \leq C_{ext} \leq$ 100 Mm^{-1}, and then decreased. The maximum value of α_{abs} was approximately 1.2 (Fig. 11(d)). Although the value of C_{ext} at which α_{abs} was maximized in Fukuoka differed from that in Beijing, the maximum values of α_{abs} in Fukuoka and Beijing were the same. As shown in Fig. 11(d), α_{abs_sw} was always lower than α_{abs_lw}. As demonstrated by the change in α_{ext} and G, V_f decreased and V_c increased in the range of C_{ext} > 200 Mm^{-1} in Fig. 11(e).

During the spring in Fukuoka, relatively large C_{ext} values in the range of 50 to 200 Mm^{-1} were frequently observed. α_{ext} in this range was approximately 1.7. Therefore, the fraction of small particles was high. These large C_{ext} values may have been caused by air masses that did not include large particles passing over the polluted area in the continent. According to the trajectory analysis (Table 4), in the spring, the inflow of air masses passing over Japan was also high. The insolation also rapidly increased in the spring, resulting in a high aerosol production rate. This indicates that the large C_{ext} values during the spring in Fukuoka were partially caused by aerosols emitted and produced in Japan.

In the range of C_{ext} > 200 Mm^{-1}, α_{ext} was low. In Beijing, V_c was always high, and α_{ext} was low. Therefore, when C_{ext} values exceeding 200 Mm^{-1} were observed during the spring in Fukuoka, the air masses were assumed to have arrived from the heavy polluted continental area. However, the wavelength dependence of α_{abs} in Fukuoka was different from that in Beijing. Therefore, the aerosol content was modified as the air masses moved from Beijing to Fukuoka and was mixed with locally emitted aerosols.

6. Summary and conclusion

The IAP (CAS) and MRI (JMA) have been measuring aerosol optical properties as part of a cooperative Chinese and Japanese science and technology program. From 2010 to 2014, the aerosol optical characteristics in two cities (Beijing and Fukuoka) located in East Asia were measured using an integrating nephelometer and an aethalometer, and long-term season-crossing data were obtained. Using a method developed by one of the present authors, scattering coefficients measured by the nephelometer were corrected more accurately than in previous studies, and more reliable and accurate values of optical properties and their frequency distributions were obtained. The size distribution and complex index of refraction were also obtained using this method, and the relationships among the optical properties and these parameters including the α_{ext} and the α_{abs} were investigated. The results obtained in this study are summarized as follows.

The annual means of the extinction, scattering, and absorption coefficients C_{ext}

(525 nm), C_{sca} (525 nm), and C_{abs} (520 nm) and their standard deviations in Fukuoka from August 2010 to May 2014 were 74.6 ± 52.9, 66.1 ± 48.4, and 8.1 ± 5.3 Mm^{-1}, respectively, whereas those in Beijing from March 2010 to February 2014 were 412.1 ± 462.6, 367.2 ± 424.4, and 42.4 ± 37.5 Mm^{-1}, respectively. The C_{ext}, C_{sca}, and C_{abs} values in Fukuoka were approximately one-fifth of those in Beijing. The frequency distributions of C_{ext} in Fukuoka showed that C_{ext} > 500 Mm^{-1} was observed infrequently, and C_{ext} and C_{abs} were larger in the spring than in the other seasons. In Beijing, the frequency of data with C_{ext} > 1000 Mm^{-1} was relatively high. In Beijing, the frequency of C_{abs} with 10 $Mm^{-1} \leq C_{abs} \leq 60$ Mm^{-1} was high in the spring and summer. The C_{ext}, C_{sca}, and C_{abs} showed seasonal variation in both cities. Some other properties showed also seasonal variation. This seasonal variation corresponds to the variation of the characteristics of the air masses arriving in Fukuoka and Beijing.

The annual means of the SSAs ω_0 (525 nm) and their standard deviations in Fukuoka and Beijing were 0.877 ± 0.053 and 0.868 ± 0.047, respectively, and were almost equivalent. The frequency distributions of small ω_0 (525 nm) values in both cities were high in the summer. The annual means of the asymmetry factor G in Fukuoka and Beijing were 0.599 ± 0.040 and 0.656 ± 0.042, respectively. The values of G in Beijing were larger than those in Fukuoka throughout the year. The annual means of α_{ext} in Fukuoka and Beijing were 1.555 ± 0.312 and 0.855 ± 0.347, respectively. G and α_{ext} were inversely related. In Fukuoka, the volume fraction of coarse and fine mode V_f and V_c were approximately 80% and 20%, respectively. In Beijing, V_f and V_c were approximately equal except in the summer, when V_f was somewhat large. As demonstrated by the behavior of G and α_{ext}, coarse particles were present throughout the year in Beijing. The annual means of α_{abs} in Fukuoka and Beijing were 1.106 ± 0.155 and 0.977 ± 0.147, respectively. The most characteristic features is that the frequency distribution of α_{abs} demonstrates that aerosols with $\alpha_{abs} <$ 1.0 were frequently observed in both cities. This cannot be explained by the simple external mixture of absorbing aerosols such as fresh black carbon ($\alpha_{abs} \approx 1.0$), biomass burning aerosols ($\alpha_{abs} > 1.0$), and dust aerosols ($\alpha_{abs} > 1.0$). In both cities, α_{abs} showed clear seasonal variation: it was small in the summer and large in the winter.

The relationships among α_{ext}, α_{abs}, the volume size distribution and ImRf were also investigated. In both Fukuoka and Beijing, as α_{abs} decreased, V_c increased. The volume size distribution was bimodal for $\alpha_{ext} < 1$ and monomodal for $\alpha_{ext} > 1.0$. In both cities, as α_{abs} decreased, the ImRF decreased. Considering the particle size distribution, these relationships could be partially explained by internally mixed particles such as the coated sphere model. The relationships between α_{ext} and the ImRF in the two cities were similar. The difference between both cities inferred to be due to the difference in particle size distribution and aerosol compositions.

The data were roughly divided into bins according to the value of C_{ext}, and the relationships among the SSA, α_{ext}, and α_{abs} were investigated. The SSA values on the

2-dimensional table of α_{ext}, and α_{abs} showed that they depended on the particle size distribution and the aerosol compositions.

Two case studies were conducted to demonstrate the usefulness of the data. During the winter in Beijing, it was shown that as the amount of air pollution increases, the physical characteristics (particle size distribution) and optical properties of the aerosol changed. During the spring in Fukuoka, it was shown that the aerosol characteristics in the range of $C_{ext} > 200$ Mm^{-1} differed from those in the range of $C_{ext} < 200$ Mm^{-1} depending on the air mass transported.

The optical properties in Fukuoka and Beijing were investigated by simultaneously analyzing data from both locations. We were able to show some aerosol characteristics in both cities. The α_{ext} is an index of the size distribution, and the α_{abs} is dependent on the absorbing components. These parameters were useful parameters for characterizing aerosol properties. Using the data obtained in this study, more advanced data analysis can be conducted in the future with the support of meteorological data or other supplementary information. Because the optical properties of aerosols depend on their composition, mixing state, shape, and refractive index, it is necessary to simultaneously measure these parameters to understand the aerosol optical properties.

Acknowledgements

This study was conducted as part of a cooperative Chinese and Japanese science and technology program. The work was supported by the National Natural Science Foundation of China (Grant Nos. 41475136 and 41590871), the International Science & Technology Cooperation Program of China (No. 2013DFG22820), and the Beijing Open Research Fund of Jiangsu Provincial Meteorological Bureau. It was partially supported by Japan Society for the Promotion of Science (JSPS) Grants-in-Aid for Scientific Research (Nos. 19340139 and 22310015). The authors would also like to thank Dr. Hara and Dr. Shiraishi of Fukuoka University for their support in obtaining measurements and maintaining instruments and three anonymous reviewers for their useful comments. Furthermore, we would like to express our appreciation to Dr. Kuji, the editor in charge of this paper. His detailed comments aided in the significant improvement of this paper.

References

Anderson, T. L., D. S. Covert, S. F. Marshall, M. L. Laucks, R. J. Charlson, A. P. Waggoner, J. A. Ogren, R. Caldow, R. L. Holm, F. R. Quant, G. J. Sem, A. Wiedensohler, N. A. Ahlquist, and T. S. Bates, 1996: Performance characteristics of a high-sensitivity, three-wavelength, total scatter/backscatter nephelometer. *J. Atmos. Ocean. Tech.*, **13**, 967–986.

Anderson, T. L., and J. A. Ogren, 1998: Determining aerosol radiative properties using the TSI 3563 integrating nephelometer. *Aerosol Sci. Technol.*, **29**, 57–69.

Arnott, W. P., H. Moosmüller, C. F. Rogers, T. Jin, and R. Bruch, 1999: Photoacoustic spectrometer for measuring light absorption by aerosol: instrument description. Atmos. Environ., 33, 2845–2852.

Arnott, W., K. Hamasha, H. Moosmüller, P. J. Sheridan and J. A. Ogren, 2005: Towards aerosol light-absorption measurements with a 7-wavelength aethalometer: Evaluation with a photoacoustic instrument and 3-wavelength nephelometer, *Aerosol Sci. Tech.*, **39**, 17–29.

Bergin, M. H., G. R. Cass, J. Xu, C. Fang, L. M. Zeng, T. Yu, L. G. Salmon, C. S. Kiang, X. Y. Tang, Y. H. Zhang, W. L. Chameides, 2001: Aerosol radiative, physical, and chemical properties in Beijing during June 1999, *J. Geophys. Res.*, **106**, 17969–17980.

Bergstrom, R.W., P. Pilewskie, P. B. Russell, J. Redemann, T. C. Bond, P. K. Quinn, and B. Sierau, 2007: Spectral absorption properties of atmospheric aerosols, *Atmos. Chem. Phys*., **7**, 5937–5943.

Bond, T. C., T. L. Anderson and D. Campbell, 1999: Calibration and intercomparison of filter-based measurements of visible light absorption by aerosols, *Aerosol Sci. Tech*., **30**, 582–600.

Bond, T. C., D. S. Covert, and T. Müller, 2009: Truncation and angular-scattering corrections for absorbing aerosol in the TSI 3563 nephelometer. *Aerosol Sci. Technol*., **43**, 866-871.

Che, H., G. Shi, H. Zhao, T. Nakajima, P. Khatri, T. Takamura, H. Wang, Y. Wang, J. Sun, and X. Zhang, 2014: Aerosol optical properties retrieved from a Prede sky radiometer over an urban site of Beijing, China. *J. Meteor. Soc. Japan*, **92A**, 17-31.

Clarke, A., C. Naughton, V. Kapustin, Y. Shinozuka, S. Howell, J. Dibb, J. Zhou, B. Anderson, V. Brekhovskikh, H. Turner, and M. Pinkerton, 2007: Biomass Burning and Pollution Aerosol over North America: Organic Components and their influence on Spectral Optical Properties and Humidification Response, *J. Geophys. Res.*, **112**, D12S18, doi:10.1029/2006JD007777.

Coen, M. Collaud, E.Weingartner, A. Apituley, D. Ceburnis, R. Fierz-Schmidhauser, H. Flentje, J. S. Henzing, S. G. Jennings, M. Moerman, A. Petzold, O. Schmid, and U. Baltensperger, 2010: Minimizing light absorption measurement artifacts of the Aethalometer: evaluation of five correction algorithms, *Atmos. Meas. Tech.*, **3**, 457–474.

Delene D. J., and J. A. Ogren, 2002: Variability of Aerosol Optical Properties at Four North American Surface Monitoring Sites. *J. Atmos. Sci.*, **59**, 1135–1150.

Draxler, R.R., 1999, HYSPLIT_4 User's Guide, NOAA Technical Memorandum ERL ARL-230, June, 35 pp.

Garland, R. M., O. Schmid, A. Nowak, P. Achtert, A. Wiedensohler, S. S. Gunthe, N. Takegawa, K. Kita, Y. Kondo, M. Hu, M. Shao, L. M. Zeng, T. Zhu, M. O.

Andreae, and U. Pöschl, 2009: Aerosol optical properties observed during Campaign of Air Quality Research in Beijing 2006 (CAREBeijing-2006): Characteristic differences between the inflow and outflow of Beijing city air, *J. Geophys. Res.*, **114**, D00G04, doi:10.1029/2008JD010780.

Gyawali, M., W. P. Arnott, K. Lewis, and H. Moosmüller, 2009 : In situ aerosol optics in Reno, NV, USA during and after the summer 2008 California wildfires and the influence of absorbing and non-absorbing organic coatings on spectral light absorption, *Atmos. Chem. Phys.*, **9**, 8007–8015.

He, X., C. C. Li, A. K. H. Lau, Z. Z. Deng, J. T. Mao, M. H. Wang, and X. Y. Liu, 2009: An intensive study of aerosol optical properties in Beijing urban area, *Atmos. Chem. Phys*., **9**, 8903–8915.

Heintzenberg, J., and R. J. Charlson, 1996: Design and applications of the integrating nephelometer: A Review. *J. Atmos. Ocean. Technol.*, **13**, 987-1000.

Li, C., L. T. Marufu, R. R. Dickerson, Z. Li, T. Wen, Y. Wang, P. Wang, H. Chen, and J.W. Stehr, 2007, In situ measurements of trace gases and aerosol optical properties at a rural site in northern China during East Asian Study of Tropospheric Aerosols: An International Regional Experiment 2005, *J. Geophys. Res*., **112**, D22S04, doi:10.1029/2006JD007592.

Liousse, C., H. Cachier, and S. G. Jennings, 1993: Optical and thermal measurements of black carbon aerosol content in different environments: Variation of the specific attenuation cross-section, sigma (σ), *Atmos. Environ.*, **27**, 1203–1211.

Lohmann, U., and J. Feichter, 2005: Global indirect aerosol effects: a review. *Atmos. Chem. Phys.*, **5**, 715-737.

McComiskey, A., E. Andrews, D. Jackson, A. Jefferson, S. W. Kim, J. Ogren, P. Sheridan, and J. Wendell, 2004: Climate Monitoring and Diagnostics Laboratory Summary Report, Summary Rep. No. 27 2002 – 2003, edited by R. C. Schnell, U.S. Dep. of Commerce, Washington, D. C., 58 – 96.

Moosmüller, H., Chakrabarty, R. K., and Arnott, W. P., 2009: Aerosol light absorption and its measurement: A review, *J. Quant. Spectrosc. Radiative transfer*, **110**, 844–878.

Müller, T., A. Nowak, A. Wiedensohler, P. Sheridan, M. Laborde, D. S. Covert, A. Marinoni, K. Imre, B. Henzing, J.-C. Roger, S. M. dos Santos, R. Wilhelm, Y.-Q. Wang, and G. de Leeuw, 2009: Angular illumination and truncation of three different integrating nephelometers: implications for empirical, size-based corrections. *Aerosol Sci. Technol.*, **43**, 581-586.

Petzold, A., C. Kopp, and R. Niessner, 1997: The dependence of the specific attenuation cross-section on black carbon mass fraction and particle size, *Atmos. Environ.*, **31**, 661–672.

Ramanathan, V., P. J. Crutzen, J. T. Kiehl, and D. Rosenfeld, 2001: Aerosols, Climate, and the Hydrological Cycle. *Science*, **294**, 2119-2124.

Roden, C. A., T. C. Bond, S. Conway, A. Benhamin, and O. Pinel, 2006: Emission factors and real-time optical properties of particles emitted from traditional wood burning cookstoves, *Environ. Sci. Technol.*, **40**, 6750–6757.

Russell, P. B., R. W. Bergstrom, Y. Shinozuka, A. D. Clarke, P. F. DeCarlo, J. L. Jimenez, J. M. Livingston, J. Redemann, O. Dubovik, and A. Strawa, 2010: Absorption Angstrom Exponent in AERONET and related data as an indicator of aerosol composition. *Atmos. Chem. Phys*., **10**, 1155-1169.

Schmid, O., P. Artaxo, W. P. Arnott, D. Chand, L. V. Gatti, G. P. Frank, A. Hoffer, M. Schnaiter, and M. O. Andreae, 2006: Spectral light absorption by ambient aerosols influenced by biomass burning in the Amazon Basin. I: Comparison and field calibration of absorption measurement techniques, *Atmos. Chem. Phys*., **6**, 3443–3462, http://www.atmos-chem-phys.net/6/3443/2006/.

Sedlacek, A., and J. Lee, 2007: Photothermal interferometric aerosol absorption spectrometry. *Aerosol Sci. Technol.*, **41**, 1089-1101.

Sheridan, P. J., D. J. Delene, and J. A. Ogren, 2001: Four years of continuous surface aerosol measurements from the Department of Energy's Atmospheric Radiation Measurement Program Southern Great Plains Cloud and Radiation Testbed site. *J. Geophys. Res*., **106**, D18, 20735-20747.

Subramanian, R., C. A. Roden, P. Boparai, and T. C. Bond, 2007: Yellow beads and missing particles: Trouble ahead for filter-based absorption measurements, *Aerosol Sci. Technol*., **41**, 630–637.

Uchiyama, A., 2014: Method to retrieve single-scattering properties of aerosols using multi-wavelength scattering and absorption coefficient data measured by integrating nephelometer and absorption photometer. *J. Meteorol. Soc. Japan*, **92A**, 71-91.

Uchiyama, A., A. Yamazaki, R. Kudo, E. Kobayashi, H. Togawa, and D. Uesawa, 2014: Continuous Ground-Based Observation of Aerosol Optical Properties at Tsukuba, Japan (Trend and Climatology). *J. Meteorol. Soc. Japan*, **92A**, 93-108.

Virkkula, A., T. Makela, R. Hillamo, T. Yli-Tuomi, A. Hirsikko, K. Hameri, and I. K. Koponen, 2007: A simple procedure for correcting loading effects of aethalometer data, *J. Air Waste Manage*., **57**, 1214–1222.

Weingartner, E., H. Saathof, M. Schnaiter, N. Streit, B. Bitnar, and U. Baltensperger, 2003: Absorption of light by soot particles: Determination of the absorption coefficient by means of Aethalometers, *J. Aerosol Sci*., **34**, 1445–1463.

Yamamoto, G., and M. Tanaka, 1972: Increase of Global Albedo Due to Air Pollution. *J. Atmos, Sci*., **29**, 1405-1412.

Yan, P., J. Tang, J. Huang, J.T. Mao, X. J. Zhou, Q. Liu, Z. F. Wang, and H. G. Zhou, 2008: The measurement of aerosol optical properties at a rural site in Northern China, *Atmos. Chem. Phys*., **8**, 2229–2242.

Yang, M., S. G. Howell, J. Zhuang, and B. J. Huebert, 2009: Attribution of aerosol light absorption to black carbon, brown carbon, and dust in China - interpretations of atmospheric measurements during EAST-AIRE, *Atmos. Chem. Phys*., **9**, 2035–2050.

Table titles

Table 1 Monthly and annual means of aerosol properties in Fukuoka.

Table 2 Same as Table 1 for Beijing.

Table 3 Aerosol optical properties measured in Beijing.

Table 4 Frequency with which each region had the longest resident time for air masses reaching Fukuoka. The resident time is defined as the time an air mass stays in a given region within the five days prior to it arriving in the target city. Frequencies were calculated each month after backward trajectory analysis.

Table 5 Same as Table 4 for Beijing.

Table 6 Relationships among ω_0, α_{ext}, and α_{abs} in Fukuoka.

Table 7 Same as Table 6 for Beijing.

Figure captions

Fig. 1 (a) Map of East Asia. Fukuoka, Beijing, and other large cities are shown.

(b) Map of East Asia showing the nine regions considered in backward trajectory analysis. (1) North Continent, (2) West China, (3) East China, (4) Korea, (5) East

China Sea, (6) Japan, (7) Southeast Asia, (8) West Pacific, (9) outside.

Fig. 2 Time series of monthly mean scattering and absorption coefficients with standard deviations in (a) Fukuoka and (b) Beijing. Normalized frequency distributions of extinction coefficients for every season in (c) Fukuoka and (d) Beijing. Normalized frequency distributions of absorption coefficients for every season in (e) Fukuoka and (f) Beijing. Winter, spring, summer, and autumn are defined as December–February, March–May, June–August, and September–November, respectively. The frequency distributions shown here are normalized to 1.

Fig. 3 Same as Fig. 2 for the SSA ω_0 at a wavelength of 525 nm.

Fig. 4 Same as Fig. 2 for the absorption Ångström exponent α_{abs}.

Fig. 5 Scatter plot of the extinction and absorption Ångström exponents α_{ext} and α_{abs} in (a) Fukuoka and (b) Beijing.

Fig. 6 Volume size distributions for α_{abs} bins in (a) Fukuoka and (b) Beijing. A dashed line indicates that fewer than 25 data points were obtained for that bin. The total numbers of data points in Fukuoka and Beijing are approximately 44000 and 36000, respectively.

Fig. 7 Volume size distributions for α_{ext} bins in (a) Fukuoka and (b) Beijing. Dashed lines indicate that fewer than 25 data points were obtained for that bin.

Fig. 8 Relationship between α_{abs} and ImRF in (a) Fukuoka and (b) Beijing. Dashed lines indicate bins with fewer than 25 data points.

Fig. 9 Relationship between α_{ext} and ImRF in (a) Fukuoka and (b) Beijing. Dashed lines indicate bins with fewer than 25 data points.

Fig. 10 Relationships between aerosol characteristics and the extinction coefficient during the winter in Beijing. (a) SSA at wavelengths of 450, 525, and 635 nm. (b) Asymmetry factor. (c) Extinction Ångström exponent. (d) Absorption Ångström exponents for all wavelengths, wavelengths shorter than 520 nm, and wavelengths longer than 590 nm. (e) Fine and coarse mode volume fractions.

Fig. 11 Same as 10 for the spring in Fukuoka.

Table 1 Monthly and annual means of aerosol properties in Fukuoka

Month	1	2	3	4	5	6	7	8	9	10	11	12	Annual mean
C_{ext} (525 nm)	90.4	77.7	93.0	82.7	115.3	60.9	56.6	57.3	54.2	63.7	75.9	67.3	74.6
SD	61.1	63.2	62.4	45.1	71.4	40.1	49.4	46.8	34.2	42.6	58.7	45.9	52.9
C_{sca} (525 nm)	79.8	68.5	84.2	74.1	105.6	53.8	50.6	50.5	46.0	54.9	66.8	58.6	66.1
SD	55.8	57.4	58.1	41.1	66.7	36.6	46.3	43.7	30.2	38.0	53.3	40.7	48.4
C_{abs} (520 nm)	9.9	8.5	8.8	8.4	9.5	7.0	5.6	6.2	7.6	8.7	9.0	8.3	8.1
SD	6.2	6.2	5.4	4.6	5.3	4.4	3.9	4.0	4.7	5.6	6.6	5.9	5.3
ω_0 (525 nm)	0.880	0.876	0.898	0.895	0.910	0.869	0.880	0.863	0.850	0.855	0.874	0.871	0.877
SD	0.047	0.053	0.039	0.034	0.032	0.062	0.065	0.075	0.063	0.053	0.049	0.050	0.053
G (525 nm)	0.605	0.599	0.601	0.579	0.588	0.603	0.595	0.608	0.606	0.600	0.606	0.600	0.599
SD	0.041	0.048	0.032	0.037	0.047	0.035	0.036	0.048	0.043	0.033	0.039	0.037	0.040
α_{ext}	1.509	1.509	1.543	1.724	1.641	1.514	1.574	1.491	1.499	1.565	1.524	1.564	1.555
SD	0.336	0.395	0.261	0.282	0.371	0.274	0.281	0.370	0.326	0.249	0.288	0.268	0.312
α_{abs}	1.184	1.170	1.138	1.192	1.100	1.040	0.939	0.955	1.051	1.133	1.173	1.196	1.106
SD	0.121	0.136	0.118	0.142	0.180	0.162	0.233	0.193	0.154	0.140	0.120	0.121	0.155
α_{abs_sw}	1.212	1.167	1.099	1.142	1.036	0.998	0.898	0.924	1.02	1.124	1.195	1.227	1.087
SD	0.169	0.179	0.161	0.189	0.217	0.200	0.243	0.218	0.188	0.182	0.171	0.170	0.192
α_{abs_lw}	1.216	1.213	1.198	1.256	1.176	1.110	1.014	1.029	1.109	1.176	1.203	1.225	1.161
SD	0.108	0.124	0.108	0.135	0.174	0.149	0.247	0.196	0.150	0.123	0.108	0.108	0.150
V_f	0.781	0.765	0.800	0.858	0.806	0.807	0.829	0.801	0.806	0.828	0.806	0.821	0.809
SD	0.151	0.183	0.111	0.093	0.137	0.122	0.106	0.150	0.130	0.096	0.117	0.106	0.128
V_c	0.219	0.235	0.200	0.142	0.194	0.193	0.171	0.199	0.194	0.172	0.194	0.179	0.191
SD	0.151	0.183	0.111	0.093	0.137	0.122	0.106	0.150	0.130	0.096	0.117	0.106	0.128
No. of data	3773	3333	4317	4205	4388	2713	3055	3417	4088	3431	3638	3915	

SD: standard deviation

C_{ext} (525 nm): extinction coefficient at a wavelength of 525 nm in units of Mm^{-1}

C_{sca} (525 nm): scattering coefficient at a wavelength of 525 nm in units of Mm^{-1}

C_{abs} (520 nm): absorption coefficient at a wavelength of 525 nm in units of Mm^{-1}

ω_0 (525 nm): single-scattering albedo at a wavelength of 525 nm

G (525 nm): asymmetry factor at a wavelength of 525 nm

α_{ext}: Ångström exponent for extinction coefficients

α_{abs}: Ångström exponent for absorption coefficients

α_{abs_sw}: Ångström exponent for absorption coefficients at wavelengths shorter than 520 nm

α_{abs_lw}: Ångström exponent for absorption coefficients at wavelengths longer than 520 nm

V_f: fine volume fraction (fraction of particles with radii less than 0.5 μm)

V_c: coarse volume fraction (fraction of particles with radii greater than 0.5 μm; $V_c = 1.0 - V_f$)

Annual mean is the mean of monthly means.

Table 2 Same as Table 1 for Beijing.

Month	1	2	3	4	5	6	7	8	9	10	11	12	Annual mean
C_{ext} (525 nm)	359.6	894.6	365.6	291.2	277.0	393.7	317.8	193.4	381.6	646.1	427.5	396.9	412.1
SD	385.9	921.9	409.9	300.6	231.7	322.0	240.7	164.2	354.1	709.8	459.6	477.3	462.6
C_{sca} (525 nm)	317.6	820.9	326.6	258.7	245.7	354.6	285.9	162.2	337.1	583.8	373.0	340.1	367.2
SD	347.1	854.9	374.9	274.9	213.0	301.2	227.6	145.7	323.1	661.0	411.5	417.2	424.4
C_{abs} (520 nm)	39.9	66.5	38.8	30.9	30.4	38.3	31.7	30.4	42.0	59.8	52.1	48.1	42.4
SD	38.4	58.3	37.2	25.2	20.6	23.4	18.3	19.6	30.5	50.0	49.1	49.2	37.5
ω_0 (525 nm)	0.873	0.904	0.877	0.873	0.871	0.879	0.879	0.811	0.861	0.871	0.855	0.856	0.868
SD	0.031	0.028	0.037	0.044	0.051	0.045	0.059	0.069	0.051	0.049	0.042	0.038	0.047
G (525 nm)	0.654	0.647	0.656	0.654	0.664	0.667	0.670	0.646	0.662	0.661	0.645	0.648	0.656
SD	0.034	0.044	0.047	0.051	0.045	0.043	0.038	0.044	0.030	0.035	0.040	0.043	0.042
α_{ext}	0.742	0.889	0.896	0.912	0.895	0.882	0.796	0.992	0.904	0.860	0.781	0.716	0.855
SD	0.269	0.420	0.376	0.399	0.419	0.367	0.388	0.365	0.258	0.232	0.318	0.275	0.347
α_{abs}	1.118	1.199	1.060	0.993	0.933	0.867	0.815	0.860	0.867	0.923	1.023	1.068	0.977
SD	0.145	0.171	0.145	0.154	0.148	0.143	0.163	0.138	0.135	0.153	0.135	0.129	0.147
α_{abs_sw}	1.242	1.312	1.126	1.007	0.899	0.815	0.754	0.810	0.830	0.925	1.092	1.180	0.999
SD	0.253	0.293	0.212	0.200	0.179	0.163	0.193	0.151	0.168	0.195	0.202	0.219	0.206
α_{abs_lw}	1.093	1.181	1.048	1.001	0.962	0.913	0.863	0.903	0.904	0.941	1.016	1.047	0.989
SD	0.106	0.115	0.125	0.140	0.136	0.138	0.152	0.133	0.121	0.134	0.117	0.104	0.128
V_f	0.401	0.442	0.506	0.455	0.488	0.463	0.457	0.522	0.438	0.388	0.413	0.401	0.448
SD	0.212	0.274	0.254	0.236	0.226	0.220	0.239	0.231	0.185	0.189	0.232	0.230	0.229
V_c	0.599	0.558	0.494	0.545	0.512	0.537	0.543	0.478	0.562	0.612	0.587	0.599	0.552
SD	0.212	0.274	0.254	0.236	0.226	0.220	0.239	0.231	0.185	0.189	0.232	0.230	0.229
No. of data	2480	2437	3497	2998	4257	4640	3952	2468	2859	3051	2356	2323	

Table 3 Aerosol optical properties measured in Beijing

Site	Period	*Csca*	*Cabs*	SSA	Instrumentation	Reference
PKU, Beijing	1 week in June 1999	488 ± 40 (530 nm)	83 ± 40 (565 nm)	0.81 ± 0.08 (550 nm)	PSAP, M903	Bergin et al. (2001)
SDZ, Beijing (rural)	September 2003 – January 2005	174.6 ± 189.1 (525 nm)	17.54 ± 3.44 (525 nm)	0.88 (550 nm)	AE31, M9003	Yan et al. (2009)
Beijing (rural)	March 2005	468 ± 472 (550 nm)	65 ± 75 (550 nm)	0.81–0.85	PSAP, TSI Model 3563	Li et al. (2007)
Beijing (rural)	11 August – 9 September 2006	361 ± 295 (550 nm)	51.8 ± 36.5 (532 nm)	0.86 ± 0.07	PAS, TSI Model 3563	Garland et al. (2009)
PKU, Beijing	January 2005 – December 2006	288 ± 281 (525 nm)	56 ± 49 (532 nm)	0.80 ± 0.09 (525 nm)	AE16, M9003	He et al. (2009)
IAP, Beijing	March 2010 – February 2014	367.2 ± 424.4 (525 nm)	42.4 ± 37.5 (520 nm)	0.868 ± 0.047 (525 nm)	AE31, Aurora3000	Present study

PKU: Peking University
SDZ: Shangdianzi Global Atmosphere Watch (GAW) Regional Station
IAP: Institute of Atmospheric Physics
PSAP: Particle Soot Absorption Photometer (Radiance Research, USA)
M903: integrating nephelometer (Radiance Research, USA)
AE31, AE16: aethalometer (Magee Scientific, USA)
M9003: integrating nephelometer (Acoem, Australasia)
TSI Model 3563: integrating nephelometer (TSI, USA)
PAS: photoacoustic spectrometer (Desert Research Institute, USA)
Aurora 3000: integrating nephelometer (Acoem, Australasia)

Table 4 Frequency with which each region had the longest resident time for air masses reaching Fukuoka. The resident time is defined as the time an air mass stays in a given region within the five days prior to it arriving in the target city. Frequencies were calculated each month after backward trajectory analysis.

	Month	1	2	3	4	5	6	7	8	9	10	11	12	All
1	North Continent	1319	993	1049	835	389	57	4	42	275	604	973	1278	7818
2	West China	6	5	5	0	1	0	0	0	0	3	12	2	34
3	East China	143	124	147	110	106	41	116	44	38	103	172	171	1315
4	Korea	179	169	159	130	221	78	99	101	90	187	187	140	1740
5	East China Sea	36	81	135	157	239	450	480	381	101	32	70	79	2241
6	Japan	156	242	282	496	742	773	275	610	1036	886	353	146	5997
7	Southeast Asia	0	0	0	0	3	126	317	136	19	0	0	0	601
8	West Pacific Ocean	7	20	31	62	155	267	569	545	237	43	0	4	1940
9	(outside)	14	64	52	10	4	8	0	1	4	2	33	40	232
		1860	1698	1860	1800	1860	1800	1860	1860	1800	1860	1800	1860	21918

: most frequent   : second most frequent

Table 5 Same as Table 4 for Beijing.

	Month	1	2	3	4	5	6	7	8	9	10	11	12	All
1	North Continent	819	705	794	612	538	251	202	228	338	569	701	842	6599
2	West China	29	26	27	4	4	2	0	0	2	13	58	40	205
3	East China	268	288	292	449	551	711	895	867	740	534	312	224	6131
4	Korea	0	0	0	7	10	66	5	21	0	0	3	0	112
5	East China Sea	0	0	0	2	13	40	9	0	0	0	0	0	64
6	Japan	0	0	0	2	0	10	0	0	0	0	0	0	12
7	Southeast Asia	0	0	0	0	0	0	0	0	0	0	0	0	0
8	West Pacific Ocean	0	0	0	0	0	0	5	0	0	0	0	0	5
9	(outside)	0	1	3	4	0	0	0	0	0	0	6	10	24
		1116	1020	1116	1080	1116	1080	1116	1116	1080	1116	1080	1116	13152

(dark shading): most frequent (light shading): second most frequent

Table 6 Relationships among ω_0, α_{ext}, and α_{abs} in Fukuoka.
Cells where fewer than 10 data points were collected are not colored. −99 indicates no data.
The number in parentheses is the number of data. The total number of data points is approximately 44,000.

(a) C_{ext} = 1–25 Mm^{-1}

α_{abs}/α_{ext}	−0.5–0.5	0.5–1.0	1.0–1.5	1.5–2.0	2.0–2.5	2.5–3.0
0.2–0.4	0.887 (19)	0.917 (22)	0.914 (40)	0.932 (21)	0.813 (2)	−99 (0)
0.4–0.6	0.834 (50)	0.862 (48)	0.888 (40)	0.918 (25)	0.945 (2)	−99 (0)
0.6–0.8	0.843 (123)	0.798(185)	0.850 (141)	0.903 (51)	0.910 (1)	0.891 (1)
0.8–1.0	0.828 (87)	0.821 (469)	0.824 (840)	0.863 (209)	0.901 (17)	0.849 (3)
1.0–1.2	0.837 (16)	0.851 (238)	0.834 (1360)	0.841 (945)	0.876 (50)	0.695 (3)
1.2–1.4	0.841 (7)	0.854 (20)	0.850 (299)	0.840 (809)	0.835 (115)	0.819 (3)
1.4–1.6	0.743 (2)	0.922 (1)	0.844 (19)	0.847 (68)	0.829 (44)	0.720 (5)

ω_0
0.95–1.00
0.90–0.95
0.85–0.90
0.80–0.85
0.75–0.80
0.70–0.75
<0.70

(b) C_{ext} = 25–100 Mm^{-1}

α_{abs}/α_{ext}	−0.5–0.5	0.5–1.0	1.0–1.5	1.5–2.0	2.0–2.5	2.5–3.0
0.2–0.4	−99 (0)	−99 (0)	0.955 (8)	0.959 (7)	−99 (0)	−99 (0)
0.4–0.6	0.951 (5)	0.865 (6)	0.948 (32)	0.945 (80)	0.950 (15)	−99 (0)
0.6–0.8	0.908 (2)	0.892 (51)	0.931 (296)	0.934 (274)	0.945 (43)	−99 (0)
0.8–1.0	0.945 (11)	0.887 (267)	0.865 (1610)	0.900 (1436)	0.934 (111)	−99 (0)
1.0–1.2	0.928 (9)	0.908 (296)	0.865 (4143)	0.868 (6968)	0.898 (342)	−99 (0)
1.2–1.4	0.965 (1)	0.925 (43)	0.882 (975)	0.864 (6540)	0.882 (1254)	0.881 (5)
1.4–1.6	0.877 (1)	0.926 (1)	0.902 (21)	0.869 (444)	0.872 (428)	0.875 (6)

(c) C_{ext} = 100–1000 Mm^{-1}

$\alpha_{abs}/\alpha_{ext}$	−0.5–0.5	0.5–1.0	1.0–1.5	1.5–2.0	2.0–2.5	2.5–3.0
0.2–0.4	−99 (0)	−99 (0)	0.960 (1)	0.977 (2)	−99 (0)	−99 (0)
0.4–0.6	−99 (0)	−99 (0)	0.955 (21)	0.957 (58)	0.955 (3)	−99 (0)
0.6–0.8	0.891 (27)	0.940 (91)	0.946 (223)	0.947 (363)	0.962 (7)	−99 (0)
0.8–1.0	0.926 (31)	0.919 (394)	0.925 (1197)	0.927 (842)	0.937 (11)	−99 (0)
1.0–1.2	0.934 (39)	0.925 (298)	0.906 (2564)	0.896 (3086)	0.917 (71)	−99 (0)
1.2–1.4	0.933 (13)	0.943 (33)	0.901 (337)	0.884 (2203)	0.886 (131)	−99 (0)
1.4–1.6	0.953 (12)	0.953 (4)	0.901 (5)	0.882 (119)	0.879 (45)	−99 (0)

(d) C_{ext} = 1000–5000 Mm^{-1}

$\alpha_{abs}/\alpha_{ext}$	−0.5–0.5	0.5–1.0	1.0–1.5	1.5–2.0	2.0–2.5	2.5–3.0
0.2–0.4	−99 (0)	−99 (0)	−99 (0)	−99 (0)	−99 (0)	−99 (0)
0.4–0.6	−99 (0)	−99 (0)	−99 (0)	−99 (0)	−99 (0)	−99 (0)
0.6–0.8	−99 (0)	−99 (0)	−99 (0)	−99 (0)	−99 (0)	−99 (0)
0.8–1.0	−99 (0)	−99 (0)	−99 (0)	−99 (0)	−99 (0)	−99 (0)
1.0–1.2	0.873 (1)	−99 (0)	−99 (0)	−99 (0)	−99 (0)	−99 (0)
1.2–1.4	−99 (0)	−99 (0)	−99 (0)	−99 (0)	−99 (0)	−99 (0)
1.4–1.6	−99 (0)	−99 (0)	−99 (0)	−99 (0)	−99 (0)	−99 (0)

Table 7 Same as Table 6 for Beijing.
Cells where fewer than 10 data points were collected are not colored. −99 indicates no data.
The number in parentheses is the number of data. The total number of data points is approximately 36,000.

(a) C_{ext} = 1–25 Mm^{-1}

$\alpha_{abs}/\alpha_{ext}$	−0.5–0.5	0.5–1.0	1.0–1.5	1.5–2.0	2.0–2.5	2.5–3.0
0.2–0.4	0.855 (7)	−99 (0)	−99 (0)	−99 (0)	−99 (0)	−99 (0)
0.4–0.6	0.824 (36)	0.768 (16)	−99 (0)	−99 (0)	−99 (0)	−99 (0)
0.6–0.8	0.842 (106)	0.773 (70)	0.828 (8)	−99 (0)	−99 (0)	−99 (0)
0.8–1.0	0.852 (103)	0.809 (146)	0.853 (12)	−99 (0)	−99 (0)	−99 (0)
1.0–1.2	0.859 (31)	0.835 (41)	0.855 (22)	−99 (0)	−99 (0)	−99 (0)
1.2–1.4	0.904 (6)	0.799 (3)	0.852 (3)	−99 (0)	−99 (0)	−99 (0)
1.4–1.6	0.911 (2)	0.869 (1)	0.886 (1)	−99 (0)	−99 (0)	−99 (0)

ω_0
0.95−1.00
0.90–0.95
0.85–0.90
0.80–0.85
0.75–0.80
0.70–0.75
<0.70

(b) C_{ext} = 25–100 Mm^{-1}

$\alpha_{abs}/\alpha_{ext}$	−0.5–0.5	0.5–1.0	1.0–1.5	1.5–2.0	2.0–2.5	2.5–3.0
0.2–0.4	0.814 (8)	0.979 (1)	−99 (0)	−99 (0)	−99(0)	−99 (0)
0.4–0.6	0.845 (154)	0.851 (9)	0.765 (6)	−99 (0)	−99(0)	−99 (0)
0.6–0.8	0.854 (784)	0.814 (387)	0.798 (60)	−99 (0)	−99(0)	−99 (0)
0.8–1.0	0.869 (1278)	0.833 (1671)	0.789 (774)	0.814 (15)	−99(0)	−99 (0)
1.0–1.2	0.878 (510)	0.853 (1409)	0.815 (1062)	0.811 (78)	0.620 (1)	−99 (0)
1.2–1.4	0.892 (56)	0.865 (304)	0.854 (246)	0.807 (26)	0.700 (1)	−99 (0)
1.4–1.6	0.868 (6)	0.881 (40)	0.888 (28)	−99 (0)	−99(0)	0.717 (1)

(c) C_{ext} = 100–1000 Mm^{-1}

$\alpha_{abs}/\alpha_{ext}$	−0.5–0.5	0.5–1.0	1.0–1.5	1.5–2.0	2.0–2.5	2.5–3.0
0.2–0.4	0.843 (1)	0.923 (2)	0.958 (2)	−99 (0)	−99 (0)	−99 (0)
0.4–0.6	0.904 (73)	0.909 (87)	0.903 (18)	0.915 (2)	−99 (0)	−99 (0)
0.6–0.8	0.890 (399)	0.883 (2172)	0.875 (996)	0.865 (1)	−99 (0)	−99 (0)
0.8–1.0	0.903 (373)	0.869 (4503)	0.861 (3474)	0.831 (98)	−99 (0)	−99 (0)
1.0–1.2	0.913 (223)	0.864 (2833)	0.870 (4069)	0.836 (354)	−99 (0)	−99 (0)
1.2–1.4	0.931 (90)	0.863 (667)	0.882 (1398)	0.868 (219)	−99 (0)	−99 (0)
1.4–1.6	0.946 (43)	0.874 (58)	0.887 (185)	0.915 (42)	−99 (0)	−99 (0)

(d) C_{ext} = 1000–5000 Mm^{-1}

$\alpha_{abs}/\alpha_{ext}$	−0.5–0.5	0.5–1.0	1.0–1.5	1.5–2.0	2.0–2.5	2.5–3.0
0.2–0.4	−99 (0)	0.974 (1)	−99 (0)	−99 (0)	−99 (0)	−99 (0)
0.4–0.6	0.917 (6)	0.945 (69)	−99 (0)	−99 (0)	−99 (0)	−99 (0)
0.6–0.8	0.931 (156)	0.928 (664)	0.930 (18)	−99 (0)	−99 (0)	−99 (0)
0.8–1.0	0.925 (356)	0.915 (971)	0.907 (55)	−99 (0)	−99 (0)	−99 (0)
1.0–1.2	0.923 (249)	0.905 (814)	0.891 (259)	0.934 (1)	−99 (0)	−99 (0)
1.2–1.4	0.923 (13)	0.906 (148)	0.904 (91)	0.921 (2)	−99 (0)	−99 (0)
1.4–1.6	0.879 (1)	0.920 (7)	0.920 (17)	0.918 (8)	−99 (0)	−99 (0)

Figures

Fig.1 (a),(b)

(a)

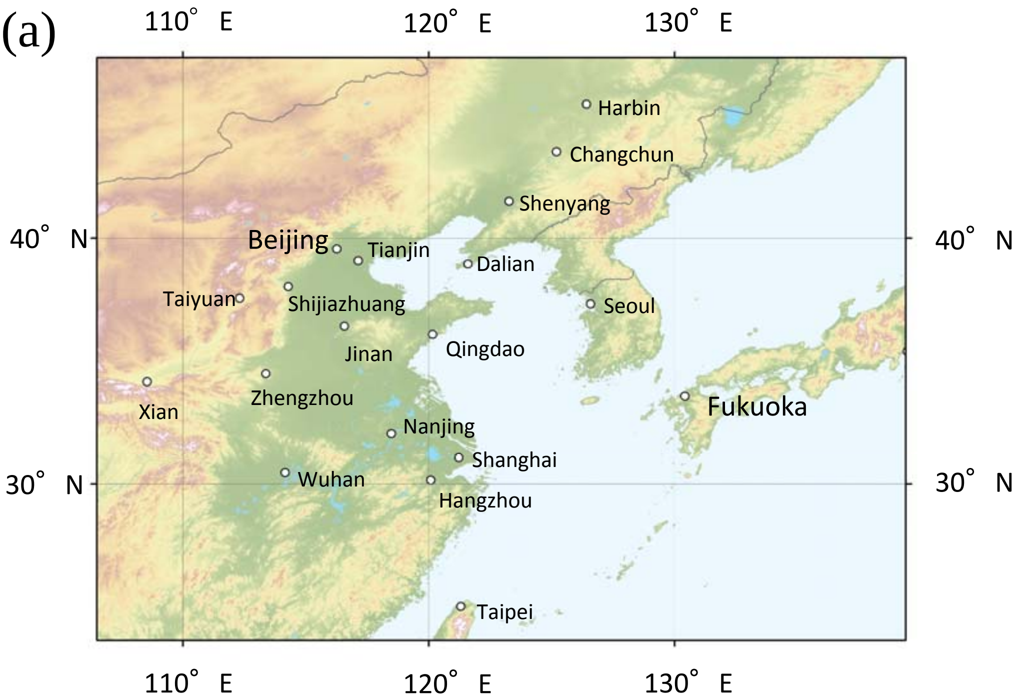
110° E
120° E
130° E
40° N
30° N
Harbin
Changchun
Shenyang
Beijing
Tianjin
Dalian
Taiyuan
Shijiazhuang
Seoul
Jinan
Qingdao
Xian
Zhengzhou
Fukuoka
Nanjing
Shanghai
Wuhan
Hangzhou
Taipei

(b)

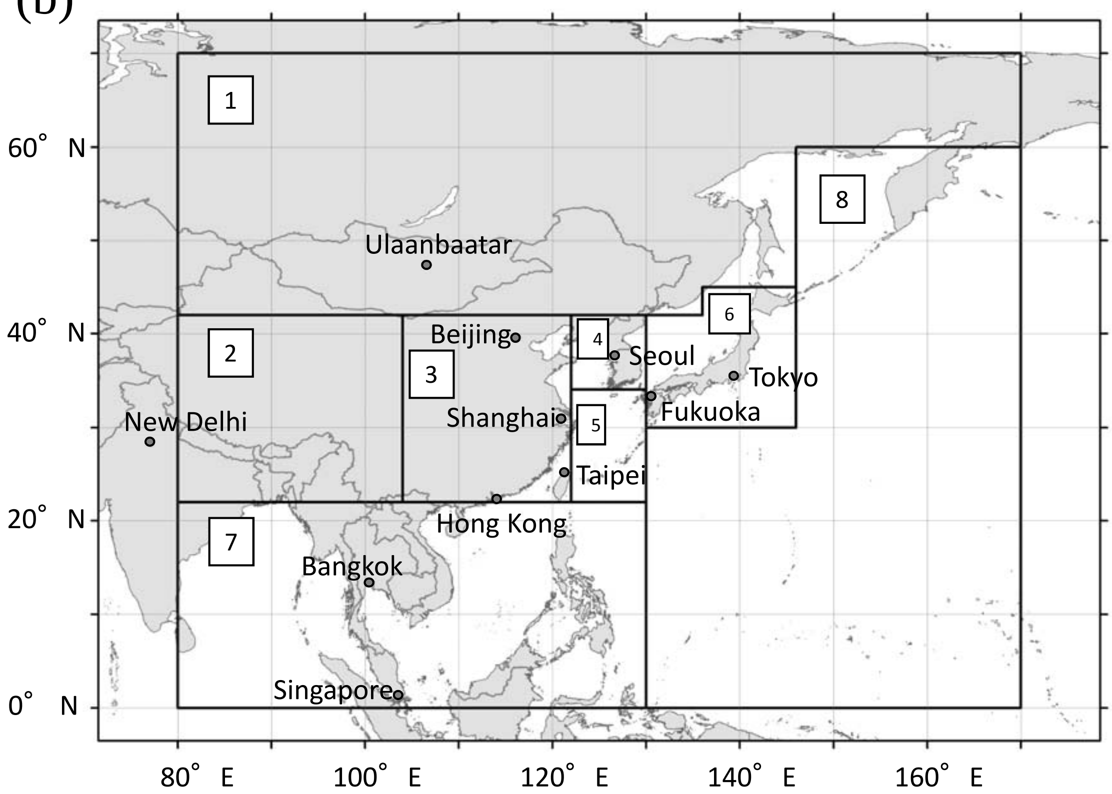
1
2
3
4
5
6
7
8
60° N
40° N
20° N
0° N
80° E
100° E
120° E
140° E
160° E
Ulaanbaatar
Beijing
Seoul
Tokyo
Fukuoka
New Delhi
Shanghai
Taipei
Hong Kong
Bangkok
Singapore

Fig. 2

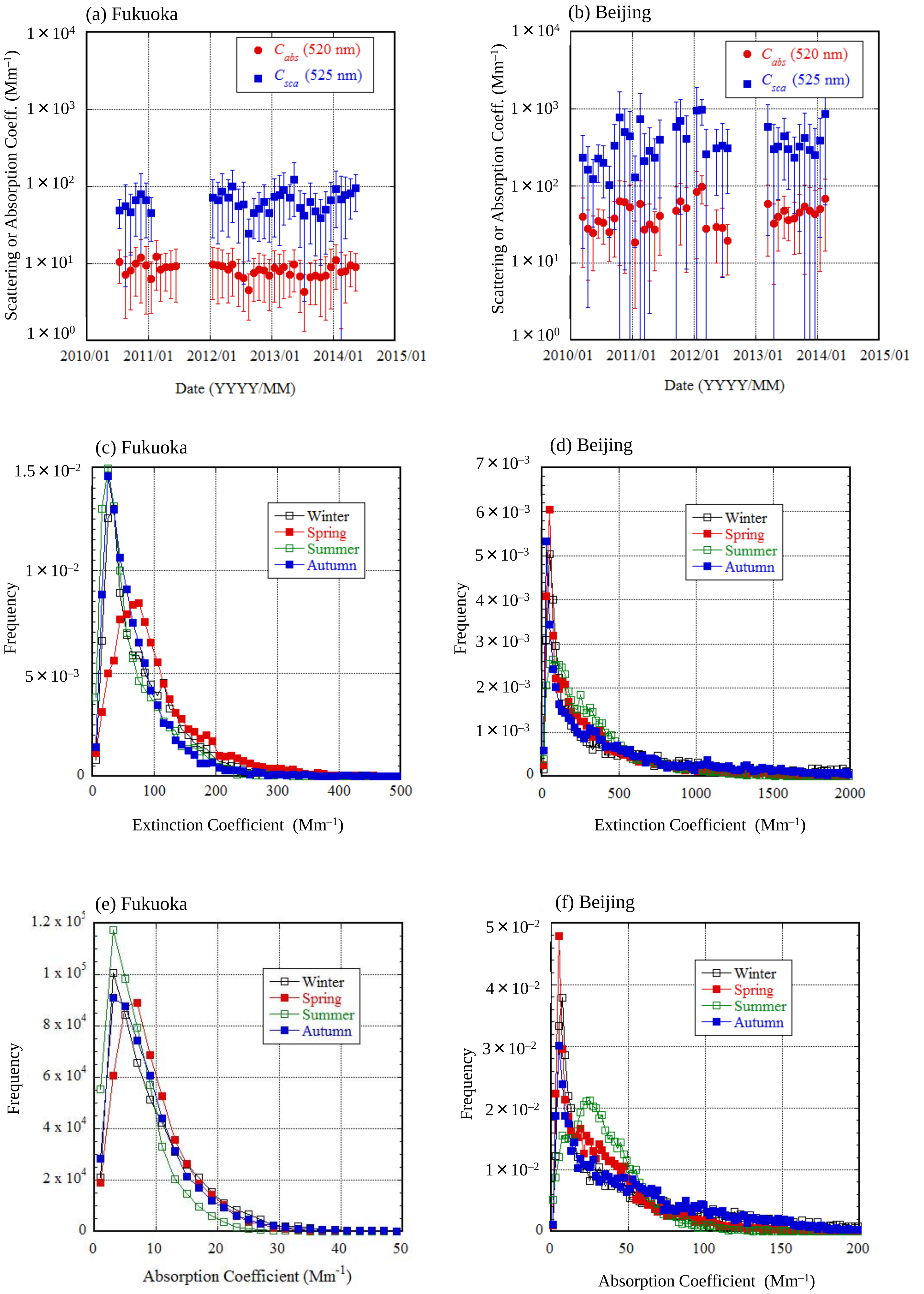

(a) Fukuoka
C_{abs} (520 nm)
C_{sca} (525 nm)
Scattering or Absorption Coeff. (Mm^{-1})
1 × 10^4
1 × 10^3
1 × 10^2
1 × 10^1
1 × 10^0
2010/01 2011/01 2012/01 2013/01 2014/01 2015/01
Date (YYYY/MM)
(b) Beijing
C_{abs} (520 nm)
C_{sca} (525 nm)
Scattering or Absorption Coeff. (Mm^{-1})
2010/01 2011/01 2012/01 2013/01 2014/01 2015/01
Date (YYYY/MM)
(c) Fukuoka
Winter
Spring
Summer
Autumn
Frequency
1.5 × 10^-2
1 × 10^-2
5 × 10^-3
0
0 100 200 300 400 500
Extinction Coefficient (Mm^{-1})
(d) Beijing
Winter
Spring
Summer
Autumn
Frequency
7 × 10^-3
6 × 10^-3
5 × 10^-3
4 × 10^-3
3 × 10^-3
2 × 10^-3
1 × 10^-3
0
0 500 1000 1500 2000
Extinction Coefficient (Mm^{-1})
(e) Fukuoka
Winter
Spring
Summer
Autumn
Frequency
1.2 x 10^5
1 x 10^5
8 x 10^4
6 x 10^4
4 x 10^4
2 x 10^4
0
0 10 20 30 40 50
Absorption Coefficient (Mm^{-1})
(f) Beijing
Winter
Spring
Summer
Autumn
Frequency
5 × 10^-2
4 × 10^-2
3 × 10^-2
2 × 10^-2
1 × 10^-2
0
0 50 100 150 200
Absorption Coefficient (Mm^{-1})

Fig. 3

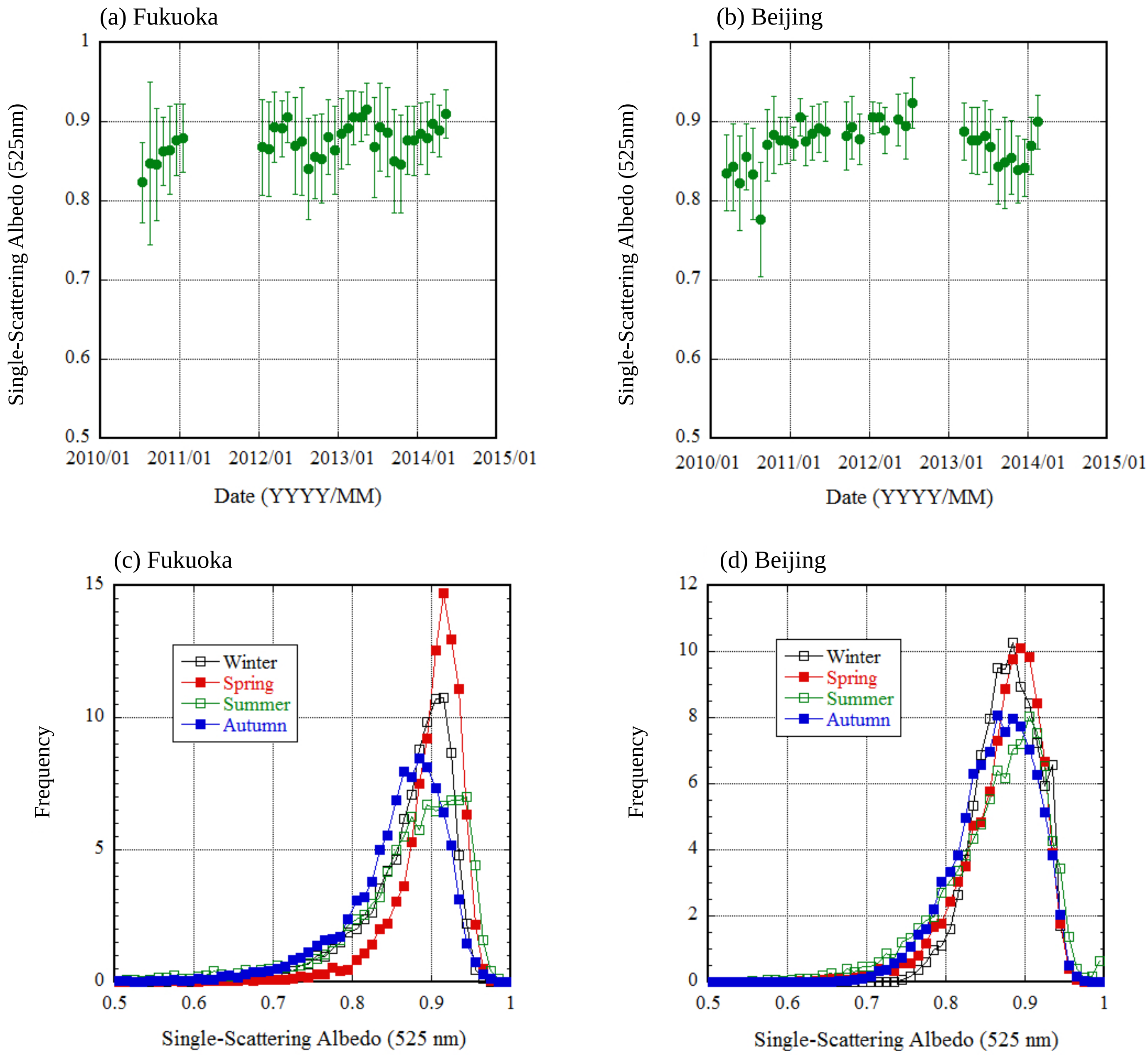
(a) Fukuoka
Single-Scattering Albedo (525nm)
Date (YYYY/MM)
2010/01
2011/01
2012/01
2013/01
2014/01
2015/01
(b) Beijing
Single-Scattering Albedo (525nm)
Date (YYYY/MM)
(c) Fukuoka
Frequency
Winter
Spring
Summer
Autumn
Single-Scattering Albedo (525 nm)
(d) Beijing
Frequency
Winter
Spring
Summer
Autumn
Single-Scattering Albedo (525 nm)

Fig. 4

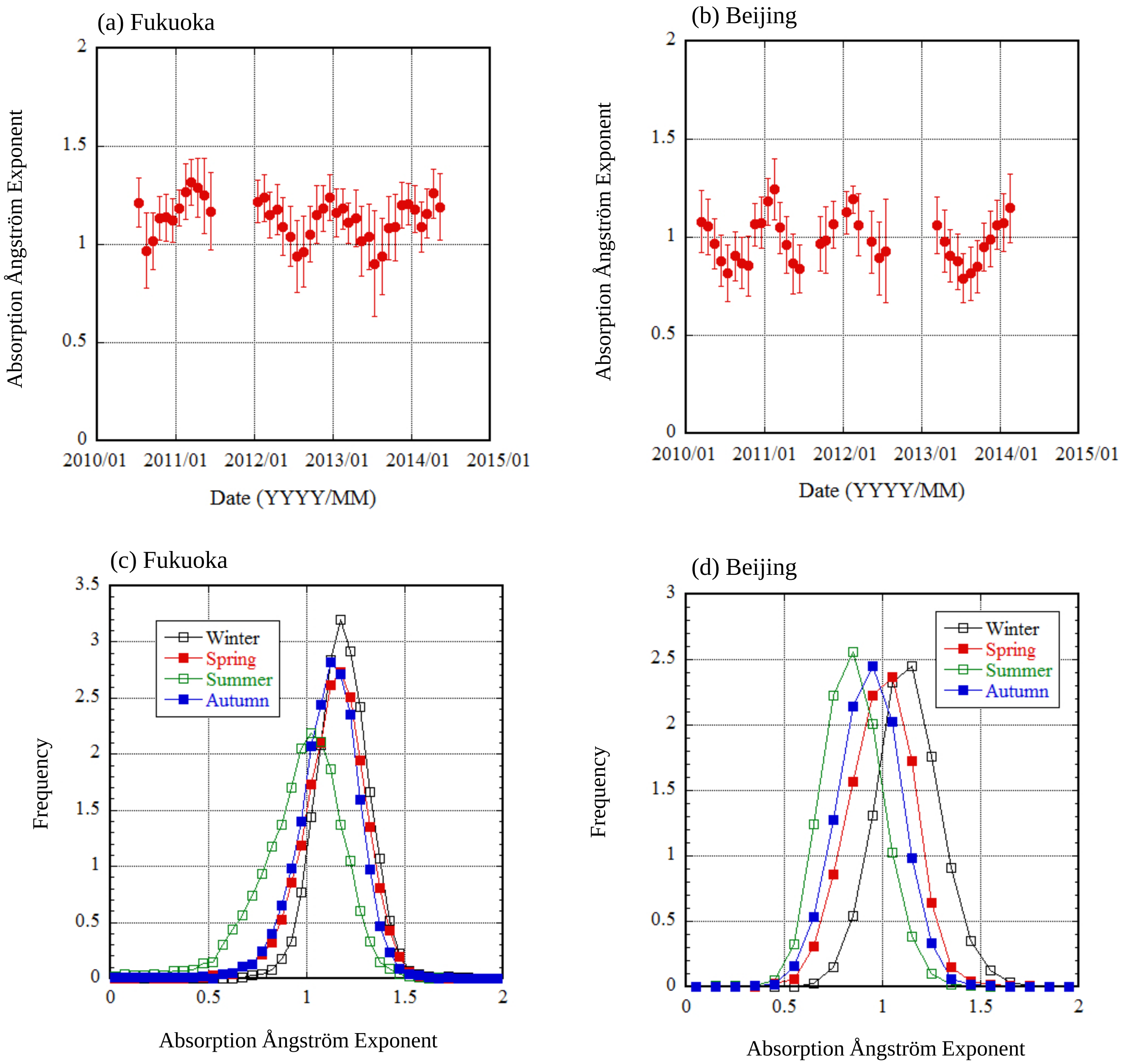

(a) Fukuoka
Absorption Ångström Exponent
0
0.5
1
1.5
2
2010/01
2011/01
2012/01
2013/01
2014/01
2015/01
Date (YYYY/MM)
(b) Beijing
Absorption Ångström Exponent
0
0.5
1
1.5
2
2010/01
2011/01
2012/01
2013/01
2014/01
2015/01
Date (YYYY/MM)
(c) Fukuoka
Frequency
0
0.5
1
1.5
2
2.5
3
3.5
Winter
Spring
Summer
Autumn
0
0.5
1
1.5
2
Absorption Ångström Exponent
(d) Beijing
Frequency
0
0.5
1
1.5
2
2.5
3
Winter
Spring
Summer
Autumn
0
0.5
1
1.5
2
Absorption Ångström Exponent

Fig. 5

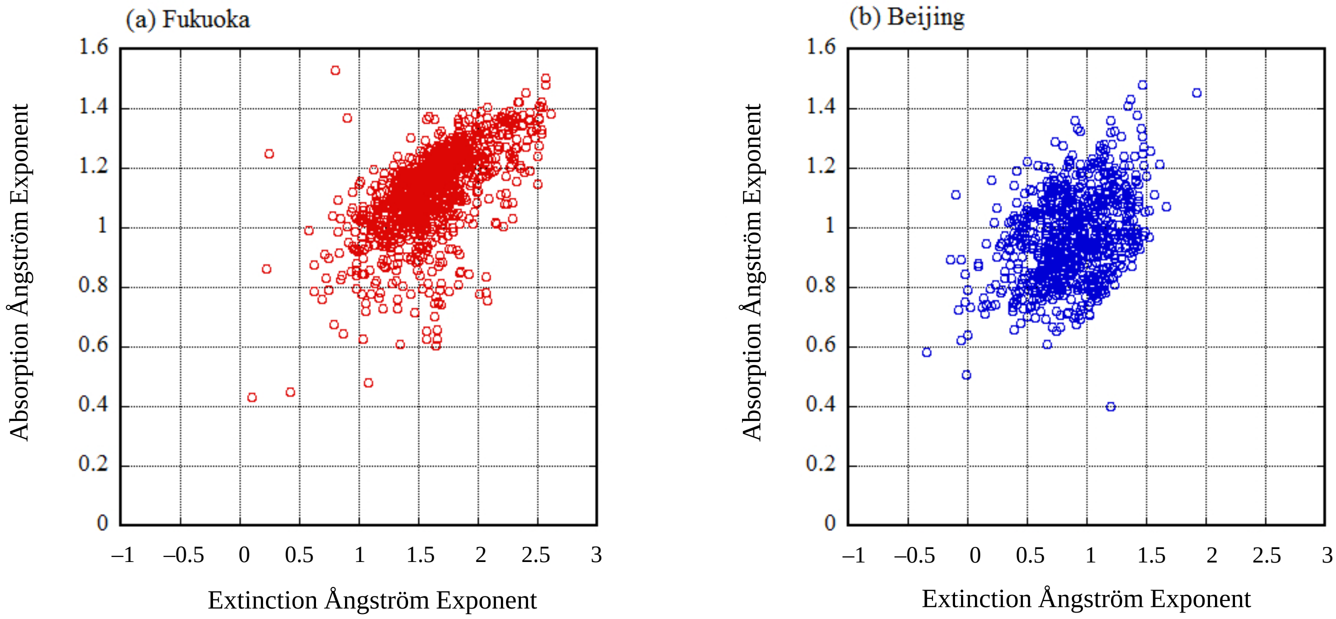
(a) Fukuoka
Absorption Ångström Exponent
Extinction Ångström Exponent
1.6
1.4
1.2
1
0.8
0.6
0.4
0.2
0
–1
–0.5
0
0.5
1
1.5
2
2.5
3
(b) Beijing
Absorption Ångström Exponent
Extinction Ångström Exponent
1.6
1.4
1.2
1
0.8
0.6
0.4
0.2
0
–1
–0.5
0
0.5
1
1.5
2
2.5
3

Fig. 6

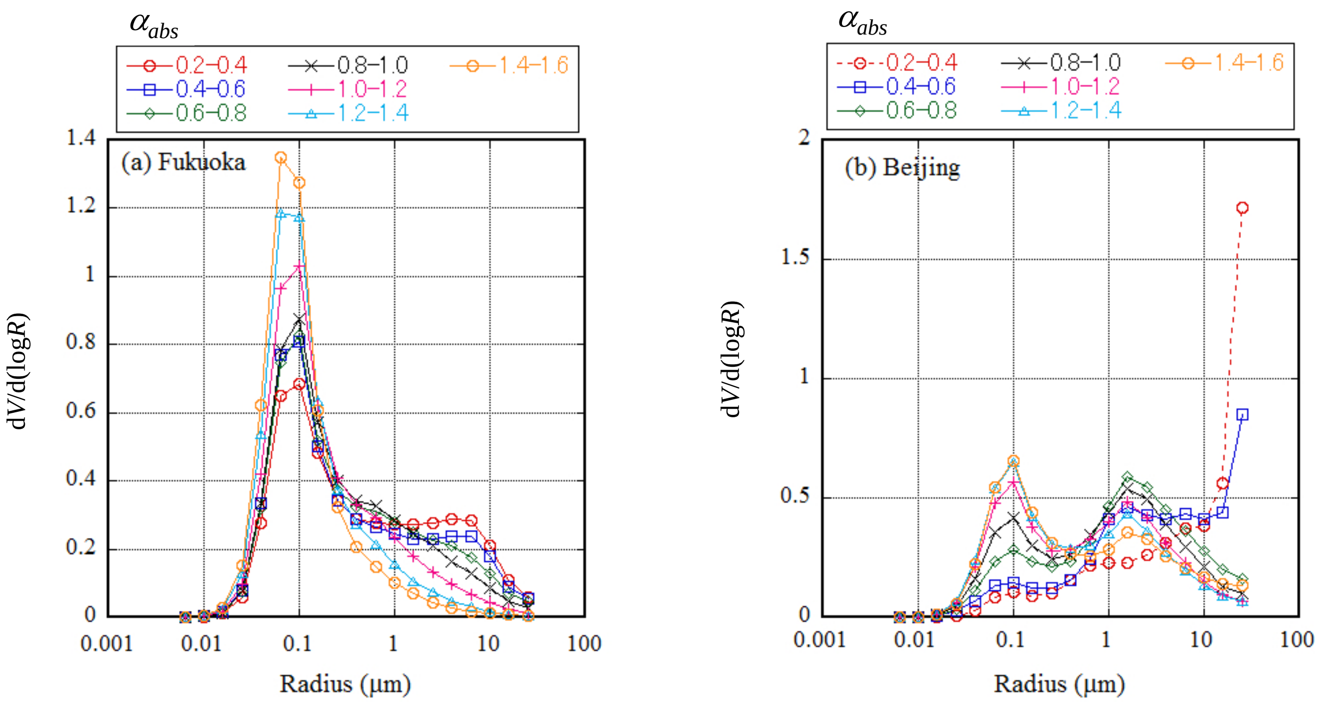

α_{abs}
0.2–0.4
0.4–0.6
0.6–0.8
0.8–1.0
1.0–1.2
1.2–1.4
1.4–1.6
(a) Fukuoka
(b) Beijing
dV/d(logR)
Radius (μm)
0.001
0.01
0.1
1
10
100

Fig. 7

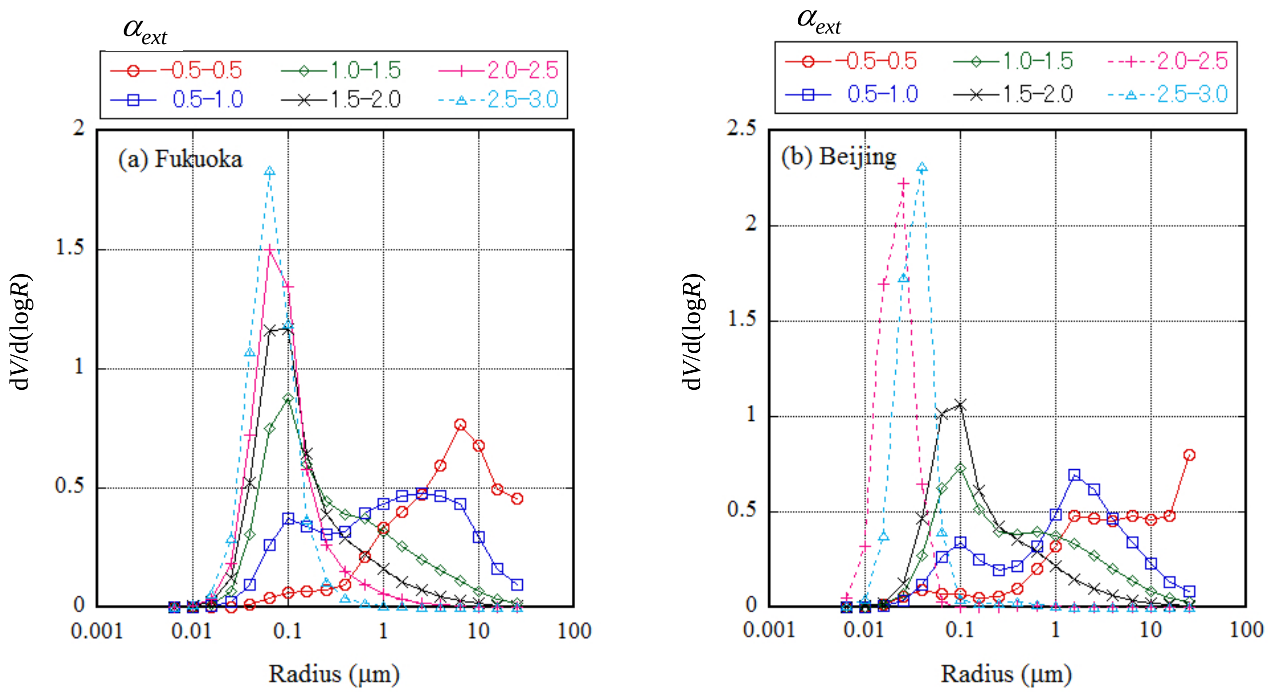

α_{ext}
-0.5–0.5
0.5–1.0
1.0–1.5
1.5–2.0
2.0–2.5
2.5–3.0
(a) Fukuoka
(b) Beijing
dV/d(logR)
Radius (μm)
0.001
0.01
0.1
1
10
100

Fig. 8

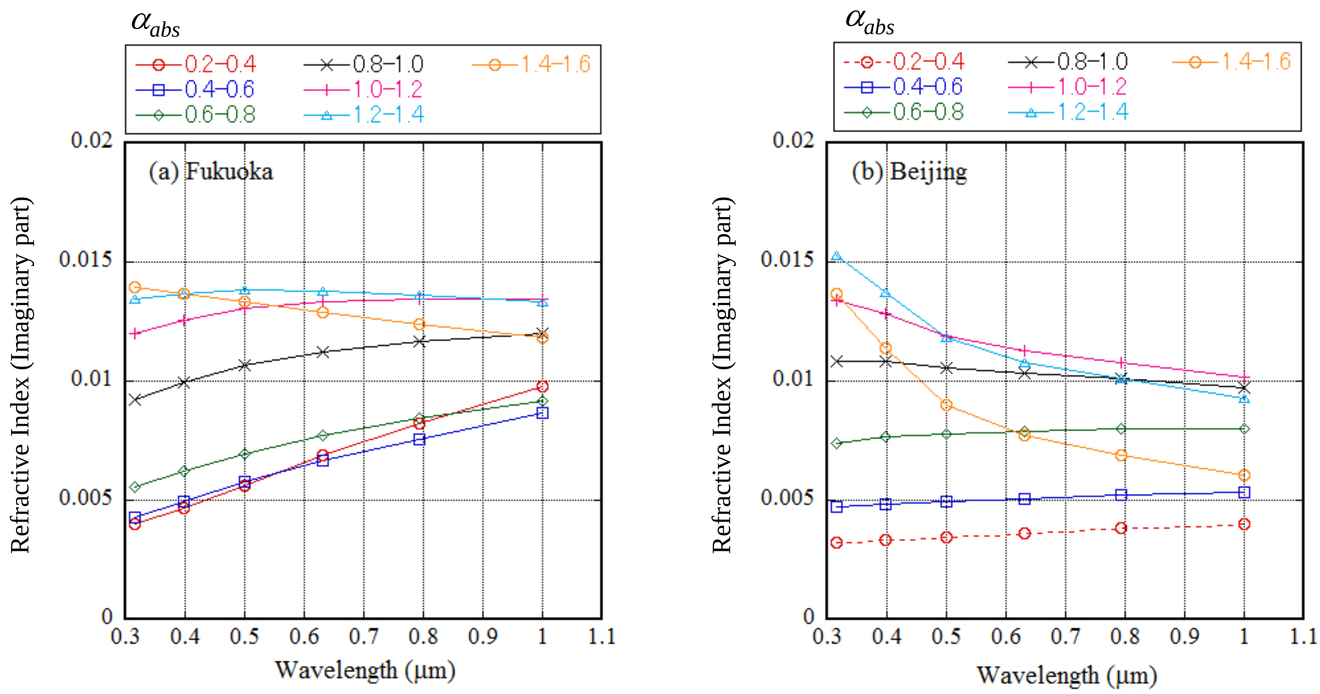

α_{abs}
0.2–0.4
0.4–0.6
0.6–0.8
0.8–1.0
1.0–1.2
1.2–1.4
1.4–1.6
(a) Fukuoka
(b) Beijing
Refractive Index (Imaginary part)
Wavelength (μm)
0
0.005
0.01
0.015
0.02
0.3
0.4
0.5
0.6
0.7
0.8
0.9
1
1.1

Fig. 9

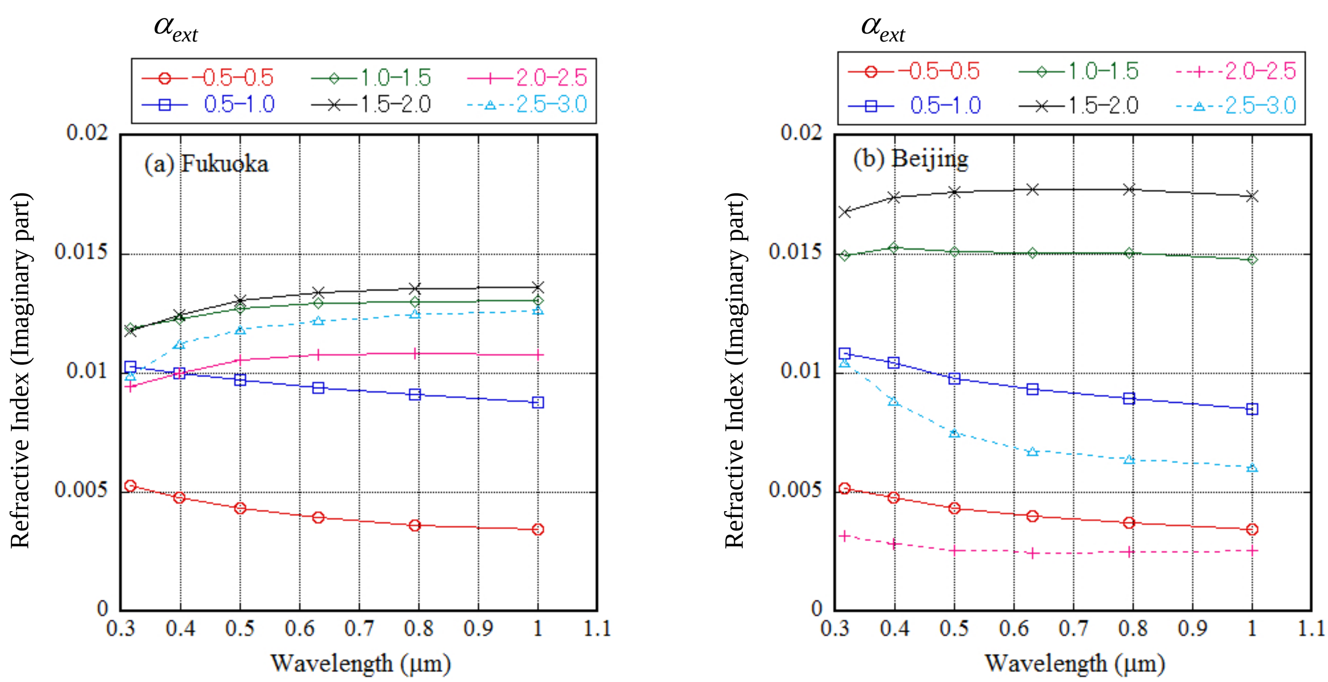

α_{ext}
−0.5–0.5
0.5–1.0
1.0–1.5
1.5–2.0
2.0–2.5
2.5–3.0
(a) Fukuoka
(b) Beijing
Refractive Index (Imaginary part)
Wavelength (μm)
0
0.005
0.01
0.015
0.02
0.3
0.4
0.5
0.6
0.7
0.8
0.9
1
1.1

Fig. 10

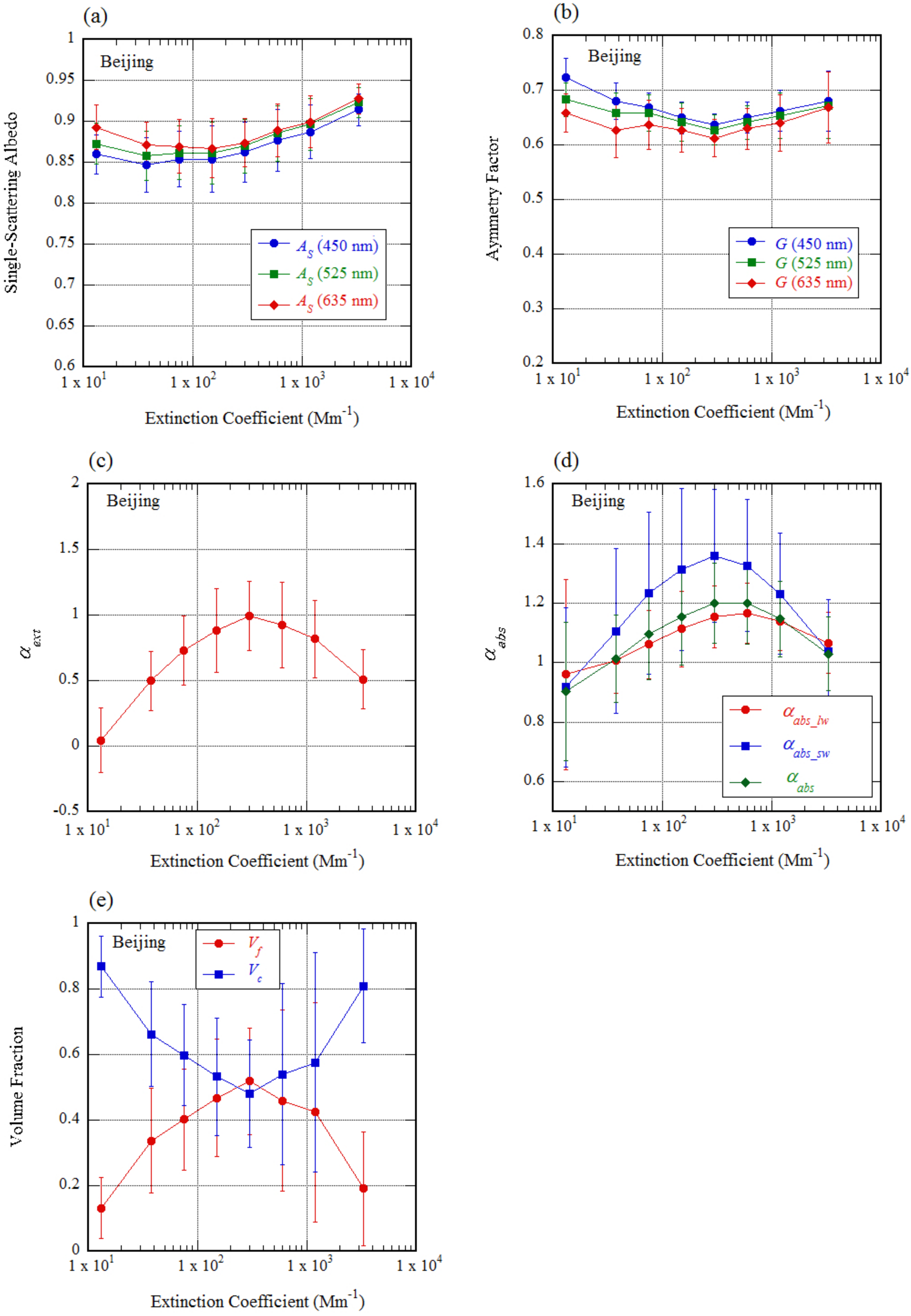
(a)
Beijing
Single-Scattering Albedo
A_S (450 nm)
A_S (525 nm)
A_S (635 nm)
1
0.95
0.9
0.85
0.8
0.75
0.7
0.65
0.6
1 x 10^1
1 x 10^2
1 x 10^3
1 x 10^4
Extinction Coefficient (Mm^{-1})
(b)
Beijing
Aymmetry Factor
G (450 nm)
G (525 nm)
G (635 nm)
0.8
0.7
0.6
0.5
0.4
0.3
0.2
1 x 10^1
1 x 10^2
1 x 10^3
1 x 10^4
Extinction Coefficient (Mm^{-1})
(c)
Beijing
α_{ext}
2
1.5
1
0.5
0
-0.5
1 x 10^1
1 x 10^2
1 x 10^3
1 x 10^4
Extinction Coefficient (Mm^{-1})
(d)
Beijing
α_{abs}
α_{abs_lw}
α_{abs_sw}
α_{abs}
1.6
1.4
1.2
1
0.8
0.6
1 x 10^1
1 x 10^2
1 x 10^3
1 x 10^4
Extinction Coefficient (Mm^{-1})
(e)
Beijing
Volume Fraction
V_f
V_c
1
0.8
0.6
0.4
0.2
0
1 x 10^1
1 x 10^2
1 x 10^3
1 x 10^4
Extinction Coefficient (Mm^{-1})

Fig. 11

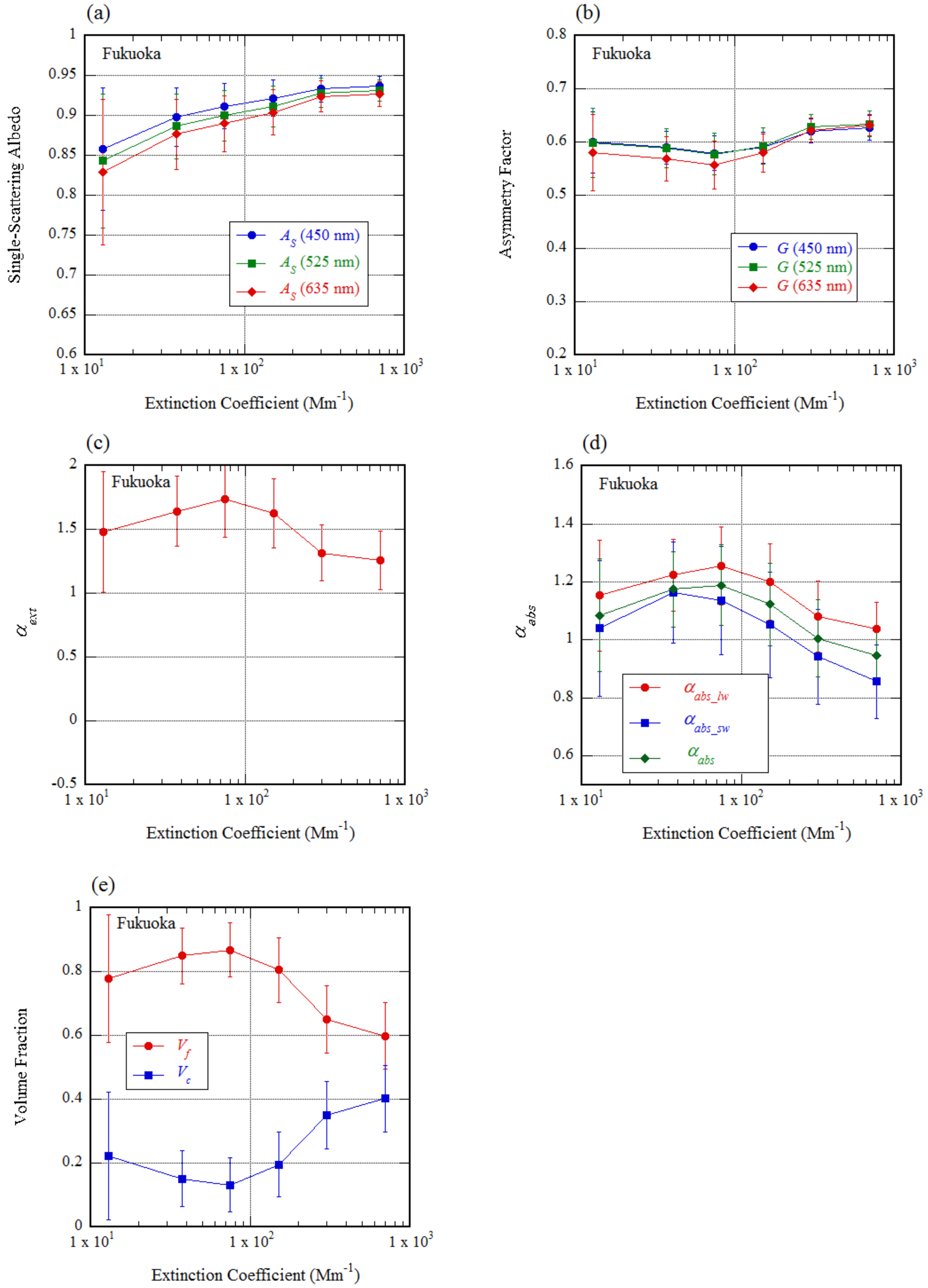

(a)
Fukuoka
Single-Scattering Albedo
1
0.95
0.9
0.85
0.8
0.75
0.7
0.65
0.6
A_S (450 nm)
A_S (525 nm)
A_S (635 nm)
1 x 10^1
1 x 10^2
1 x 10^3
Extinction Coefficient (Mm^-1)
(b)
Fukuoka
Asymmetry Factor
0.8
0.7
0.6
0.5
0.4
0.3
0.2
G (450 nm)
G (525 nm)
G (635 nm)
1 x 10^1
1 x 10^2
1 x 10^3
Extinction Coefficient (Mm^-1)
(c)
Fukuoka
α_{ext}
2
1.5
1
0.5
0
-0.5
1 x 10^1
1 x 10^2
1 x 10^3
Extinction Coefficient (Mm^-1)
(d)
Fukuoka
α_{abs}
1.6
1.4
1.2
1
0.8
0.6
α_{abs_lw}
α_{abs_sw}
α_{abs}
1 x 10^1
1 x 10^2
1 x 10^3
Extinction Coefficient (Mm^-1)
(e)
Fukuoka
Volume Fraction
1
0.8
0.6
0.4
0.2
0
V_f
V_c
1 x 10^1
1 x 10^2
1 x 10^3
Extinction Coefficient (Mm^-1)